

The Association Between VLF and ELF Chorus Emissions and Electron Precipitation

Remmy Musumpuka

A thesis submitted in fulfilment of the academic
requirements for the degree of Master of Science

in the
Space Physics Research Institute,

at the
University of KwaZulu Natal,
School of Physics,
Durban 4001,
South Africa

`rmusumpuka@yahoo.co.uk`

May 21, 2009

To my ever loving parents, Cosmas Bernard Musumpuka and Victoria Shikapwasha Musumpuka and my wonderful siblings, Cpt H. Musumpuka, Sgt C. Musumpuka, Inspector M. Musumpuka, Sr C. Musumpuka, Brenda, Bridget and Dominic. Also to my lovely lady, Namunji Kamuti, I Remmy Musumpuka final year student at the Space Physics Research Institute of the University of KwaZulu Natal in the School of Physics dedicate this Master of Science work to you all.

Preface

The experimental work described in this thesis was done at the Space Physics Research Institute in the School of Physics, University of KwaZulu-Natal, Durban, from September 2006 to December 2008, under the supervision of Professor Arthur R. W. Hughes and Dr A. B. Collier.

These studies represent original work by the author and have not otherwise been submitted in any form for any degree or diploma to any tertiary institution. Where use has been made of the work of others it is duly acknowledged in the text.

Abstract

This is an investigation into the association between ionospheric absorption caused by electron precipitation and ELF:3 Hz-3 kHz and VLF:3 kHz-30 kHz, chorus.

Ionospheric absorption was measured using the chain of riometers in Finland and related to chorus events recorded simultaneously at SANAE (L=4.2), Antarctica. The displacement in longitude of the Finnish riometers from SANAE's conjugate point made it impossible to establish a clear relationship between chorus and riometer absorption.

The diurnal variation of chorus has been established for the years 2002, 2004 and 2005 and it is shown that chorus can occur at any Local Time(LT) but has a well defined maximum probability of occurring between 0800 LT to 0900 LT.

To study the occurrence of chorus automatically we have developed an Index of ELF/VLF activity which enables us to identify chorus and distinguish it from other emissions such as hiss and whistlers.

This index of VLF Activity was established by computing the standard deviation of the VLF signal amplitude and it has been observed that the index is larger for the chorus signature as opposed to the hiss which is low and does not vary widely due to the hiss' steady signal. This index is called ASD index of "VLF Activity".

Acknowledgements

Many people contributed to the successful completion of this course, and there are several among them to whom I am exceedingly grateful. I cannot afford to mention them all but I do wish to acknowledge my two supervisors for having awarded me a scholarship through the NRF to pursue my MSc and for introducing me to Geospace physics, a highly challenging and interesting branch of physics, and whom I found dazzling in their way of reasoning, methods of research and for sending me to the most awesome places I have ever been to in the world; Professor Arthur R .W. Hughes for the patience, counsel, stimulation, friendship and for his constructive criticism and suggestions; my Co - Supervisor, Dr Andrew B. Collier for a colossal amount of help in my programming skills and data analysis, continued guidance, friendship and for making me feel at home though in a foreign land. Ann Nolte, for always having ensured that my flights, hotels and finances were organised. Adoons for being a good company and friend.

To my family, especially to my mother and father for their continued encouragements and interest in my work and for having kept me company through their phone calls. My lady Namunji for having been supportive, understanding, loving and for the phone calls, they kept me going!.

Contents

1	Introduction	1
1.1	Types of VLF Phenomena	2
1.2	Relative Ionospheric Opacity meter Absorption	3
1.3	Outline	7
2	The Magnetosphere and Ionosphere	8
2.1	Introduction	8
2.2	Magnetosphere	8
2.2.1	Trapping of Particles	11
2.3	Ionosphere	12
2.4	Collision Frequency versus Altitude	15
3	VLF Waves	16
3.1	Introduction	16
3.2	The Whistler Mode	16
3.3	Wave-Particle Interaction	20
3.3.1	Introduction	20
3.3.2	Dynamics of Energetic Charged Particles	20
3.3.3	Doppler-Shifted Cyclotron Resonance	22
3.4	Types of Emissions Observed	23
3.4.1	VLF Whistler	24
3.4.2	VLF Chorus	25
4	Chorus and Absorption	26
4.1	Introduction	26
4.2	Case studies	29
4.3	Conclusions	42

5	VLF Statistics	43
5.1	Introduction	43
5.2	VLF Chorus Statistics	44
5.3	Whistler Statistics	53
6	ASD Index of VLF Activity	57
6.1	Introduction	57
6.2	Advantages and Limitations of the Index	63
6.3	Ionospheric Absorption versus the ASD Index	64
7	Conclusion	71
7.1	Introduction	71
7.2	Discussion	72

Nomenclature

E	electric field strength
f	frequency
L	McIlwain's Parameter
R_E	mean radius of the Earth(6371 km)
n	phase refractive index
ω_p	plasma frequency
Λ	normalised frequency
ω	angular frequency
Ω	cyclotron frequency
λ	magnetic latitude
r	geocentric distance
v	velocity
B	static magnetic flux density
e	electronic charge
m	mass of a particle
v_{\parallel}	parallel velocity component
v_{\perp}	perpendicular velocity component
r_B	radius of gyration
α	pitch angle
Ω_e	electron cyclotron frequency
Φ	magnetic flux
α_{eq}	equatorial pitch angle
B_{eq}	equatorial magnetic field
α_{lc}	loss cone pitch angle

List of Figures

1.1.1 Chorus emission recorded at SANA E.	2
1.2.1 An example of QDC in gray line and the received signal in black	4
1.2.2 The location of SANA E and the Finnish chain of riometers(in red symbol)	5
1.2.3 Riometer Absorption (dB) versus Time (UT) for Abisko	6
1.2.4 Riometer Absorption (dB) versus Time (UT) for Ivalo	6
2.2.1 Schematic representation of the terrestrial magnetosphere.	10
2.3.1 The ionosphere.	14
2.4.1 Altitude variation vs collision frequency of electrons [Hanson, 1965]	15
3.2.1 Whistler ray direction	18
3.2.2 Coupling of whistler mode waves	19
3.3.2.1 Diagram illustrating the loss cone. From Roederer [1970]	22
3.3.3.1Spiral motions of electrons and whistler about the geomagnetic field.	22
3.4.1.1Spectrogram of whistlers recorded at SANA E	24
4.1.1 Illustrating the 2 methods of studying	28
4.2.1 Solar graph: Month Number versus Time(LT) [http://www.gaisma.com]	29
4.2.2 VLF quicklooks from 0330-0440UT on 17/12/04	31
4.2.3 VLF quicklooks from 0445-0600UT on 17/12/04	32
4.2.4 Riometer Absorption @ Abisko 17/12/04	33
4.2.5 VLF signal intensity from 0000-0700UT on 17/12/04	34
4.2.6 Riometer Absorption @ Ivalo 17/12/04	35
4.2.7 Riometer Absorption @ Sodankylä 17/12/04	36
4.2.8 Riometer Absorption @ Rovaniemi 17/12/04	37
4.2.9 Riometer Absorption @ Oulu 17/12/04	37
4.2.10Absorption vs L-value @ 'B' for 24/01/04	38
4.2.11VLF quicklooks from 0000-0500UT on day 275 of 2005	39

4.2.12	Absorption @ Abisko on 02/10/05	40
4.2.13	Absorption @ Ivalo on 02/10/05	40
4.2.14	Absorption @ Sodankylä on 02/10/05	41
4.2.15	Absorption @ Rovaniemi on 02/10/05	41
4.2.16	Absorption @ Oulu on 02/10/05	42
5.2.1	Schematic representation of the regions in which chorus is generated.	44
5.2.2	15:10 UT 31 January 2004	45
5.2.3	15:20 UT 31 January 2004	46
5.2.4	15:30 UT 31 January 2004	46
5.2.5	17:05 UT 31 January 2004	47
5.2.6	Diurnal and Seasonal variation of chorus for the year 2002 at SANAE	48
5.2.7	Diurnal and Seasonal variation of chorus for the year 2004 at SANAE	49
5.2.8	Diurnal and Seasonal variation of chorus for the year 2005 at SANAE	50
5.2.9	Sunspot cycle [http://science.nasa.gov/headlines/y2006/21dec_cycle24.htm]	51
5.2.10	Dst index from 2002-2005[http://spidr.ngdc.noaa.gov/spidr]	52
5.3.1	Diurnal and Seasonal Variation of whistlers for the year 2002 at SANAE	53
5.3.2	Diurnal and Seasonal Variation of whistlers for the year 2004 at SANAE	54
5.3.3	Diurnal and Seasonal Variation of whistlers for the year 2005 at SANAE	54
5.3.4	Lightning Locations http://cellar.org/showthread.php?t=800	55
6.1.1	Generating the index	58
6.1.2	Chorus averaged power spectrum	58
6.1.3	Hiss averaged power spectrum	59
6.1.4	Chorus spectrogram & its amplitude recorded at SANAE on day 59,2004	59
6.1.5	Hiss spectrogram and its amplitude recorded at SANAE on day 135,2004	60
6.1.6	ASD index of VLF activity	61
6.1.7	Chorus Case	61
6.1.8	Hiss Case	62
6.2.1	SD of VLF activity on day 275, 2005	63
6.3.1	Absorption at Abisko, vs ASD Index at SANAE on day 352,2004.	65
6.3.2	Power spectral density of the VLF signal on day 352,2004	66
6.3.3	Absorption at Ivalo, vs ASD Index at SANAE on day 352, 2004	67
6.3.4	Absorption at Sodankylä, vs ASD Index at SANAE on day 352,2004.	68
6.3.5	Absorption at Rovaniemi, vs ASD Index at SANAE on day 352,2004	69

6.3.6 Absorption at Oulu, vs ASD Index at SANAE on day 352,2004.	70
7.1 Resonant Parallel Energies vs L - value [Smith et al, 1996 Figure 10]. .	72

List of Tables

1.2.1 Finnish chain of stations at different operating frequencies and L-values.	6
4.1.1 Difference in LT and MLT from SANAE's CP for each riometer station	27
5.3.1 Monthly average, max, min hours of whistler observations at SANAE .	55
7.1 Average amplitudes of VLF emissions at different frequency bands . . .	74

Chapter 1

Introduction

The aim of this study is to investigate the association between ionospheric absorption and ELF/VLF chorus. The acronyms ELF and VLF stand for Extremely Low Frequency and Very Low Frequency which define electromagnetic frequency bands that extend from 3 Hz -30 Hz and 3 kHz - 30 kHz respectively. Absorption measurements by riometers (Relative Ionospheric Opacity meters) in Finland and ELF/VLF recordings at SANAE are used in this study. SANAE is located in the southern hemisphere at L=4.2, whereas the riometers in Finland are in longitude ranging from L=3.8 to 5.9. The location of SANAE relative to the Finnish chain is shown in Figure 1.2.2 on page 5. It should be noted that there is no station in the Finnish chain which has exactly the same L-value as SANAE. The effect of the relative location of riometers on the study is discussed in chapter 4.

It is known that in cyclotron resonance interactions energy can be exchanged between waves and particles which under certain circumstances can lead to pitch angle diffusion into the loss cone followed by electron precipitation.

Chorus, observed at SANAE, may induce electrons to precipitate in the northern hemisphere due to wave-particle resonant interactions in the equatorial plane. These electrons may produce D-region ionisation that increases ionospheric absorption which may be detected on a suitably located riometer. The D-region is a portion of the ionosphere extending from ~ 50 Km - 90 Km.

The wave-particle interaction that induces such precipitation is Doppler-shifted cyclotron resonance between VLF waves and counter-streaming electrons.

Whistler mode noise leads to electron pitch angle diffusion which results in particle precipitation into the ionosphere and creates a pitch angle distribution of trapped

particles that is unfavorable for further wave growth [Kennel and Petscheck, 1966].

1.1 Types of VLF Phenomena

Naturally occurring Very Low Frequency(VLF) electromagnetic radio waves, emanating from either the magnetosphere or from terrestrial sources, take on a variety of forms ranging from whistlers, chorus and hiss, to discrete and periodic emissions [Helliwell, 1965]. These different forms arise as a result of the properties of electromagnetic waves propagating through the magneto-ionic plasma [Walker, 1993] that surrounds the Earth. A detailed description of VLF phenomena is given in chapter 3.

Chorus is a VLF and ELF electromagnetic radio emission observed both in the magnetosphere and on the ground. Its spectral structure is made up of many discrete rising tones and sounds like the chattering of birds. Figure 1.1.1 shows an example of VLF chorus. The spectrogram shows chorus elements inter-spaced with a very clear VLF hook signature at ~ 9 seconds below 2 kHz and another one at ~ 31 seconds between 2 kHz and 3 kHz. VLF hooks are discrete emissions that are also due to cyclotron resonance between whistler mode waves and energetic electrons. The hooks evident in Figure 1.1.1 have different frequency ranges and it is possible that these are generated on different L-shells; this possibility is considered in the final chapter.

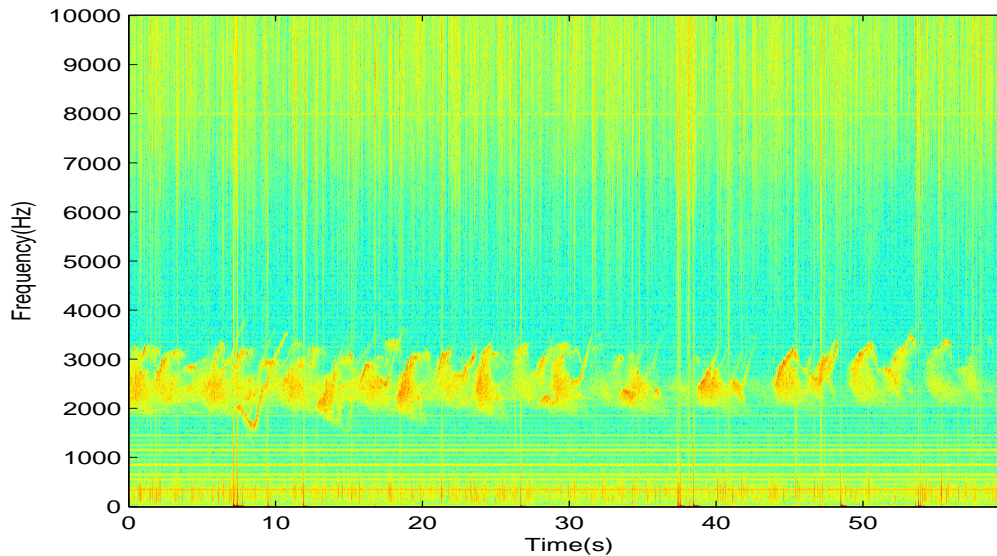


Figure 1.1.1: Chorus emission recorded at SANA E.

The starting point of most theories of chorus generation is the assumption of wave growth resulting from the Doppler-shifted cyclotron resonance interaction between whistler-mode waves and electrons [Dowden, 1962; Brice, 1963, 1964a; Kennel and Petschek, 1966; Helliwell, 1967, 1970; Helliwell and Crystal, 1973; Sudan and Ott, 1971; Matsumoto and Kimura, 1971; Nunn, 1971, 1974].

This VLF/ELF emission is generated near the equatorial plane by the transfer of energy from radiation belt electrons to whistler mode waves in the cyclotron resonance interaction [S.S Sazhin and M.Hayakawa, 1992]. It has been proposed by Trakhtengerts (1999) that there is another mechanism for the generation of chorus based on the backward wave oscillator (BWO) regime of magnetospheric cyclotron maser [Trakhtengerts, 1995; Kozelov and Tivota, 2003] but this method will not be considered in this thesis.

As a result of chorus generation, electrons are scattered in pitch angle and many of them diffuse into the loss cone and precipitate into the atmosphere [Kennel and Petschek, 1966], adding to the ionisation in the D-region of the ionosphere at altitudes of between 50 and 90 km.

1.2 Relative Ionospheric Opacity meter Absorption

Riometers measure absorption, in the ionosphere, of noise from galactic radio sources (“cosmic noise”). Riometers operate in the frequency range 25 MHz-50 MHz, well above the plasma frequency of the ionosphere. The radio waves are attenuated when there are significant numbers of free electrons and relatively high collision frequencies. This occurs at altitudes between 60 and 110 km. Riometers make continuous observation of the noise, and measure decreases relative to the quiet day level, produced by increases in ionisation.

These ground-based instruments measure the ionospheric absorption over a portion of the sky and enable us to deduce patterns of particle precipitation.

Riometer measurements are used by removing the background/cosmic signal amplitude, also called a quiet day curve (QDC) to identify absorption induced by high energy particles in lower ionosphere.

Figure 1.2.1 shows an example of the variation in received cosmic signal with respect to the quiet day curve. The difference between the received signal and the QDC at a given time is the absorption.

There are a number of methods used to determine the quiet day curve but these are

not discussed here. However, all methods essentially involve measuring the variation in cosmic noise levels in a given sidereal time interval, over a period of many days. A quiet day curve corresponds to the least amount of ionospheric cosmic radio noise absorption.

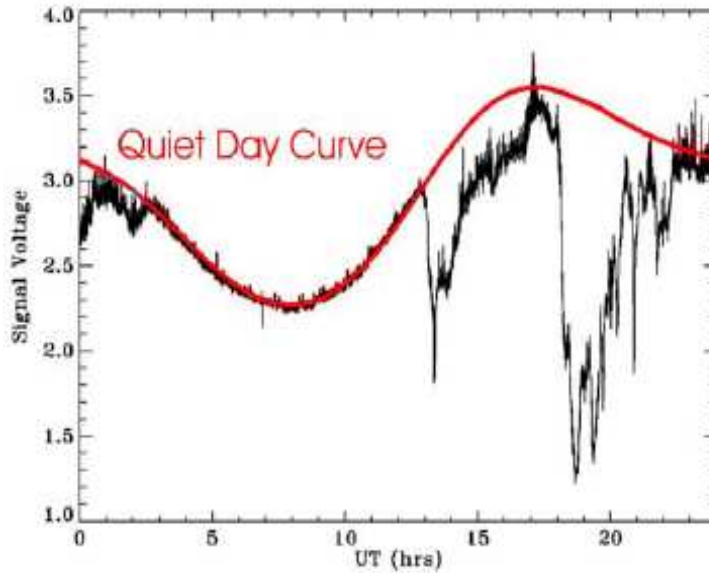


Figure 1.2.1: [[http:// www.aurora.phys.ucalgary.ca.northstar/rio/doc/CANOPUS_Riometer_Baselining.pdf](http://www.aurora.phys.ucalgary.ca.northstar/rio/doc/CANOPUS_Riometer_Baselining.pdf)]

When high-energy particles precipitate they cause deviations in the amount of cosmic radio noise that passes through the ionosphere. As these particles enter the upper atmosphere, the amount of ionisation increases. As a result, cosmic radio waves are attenuated at altitudes where the motion of electrons is collisional biased due to the increased number of free electrons. The amount of attenuation is dependent on the wave frequency and the plasma frequency. Radio waves are usually reflected if $f < f_{pmax}$, at frequencies below 20 MHz before they pass through the ionosphere, leading to a radio blackout, whilst at higher than 50 MHz, the attenuation is difficult to differentiate from its signal. Where f_{pmax} is a limiting frequency below or at which radio waves are reflected by the ionosphere. However, when frequencies between 20 MHz and 50 MHz are used, a riometer is able to monitor the “steady” signal of cosmic background, and as a result easily detects a reduction in the signal strength during particle precipitation [[http:// www.aurora.phys.ucalgary.ca.northstar/rio/doc/CANOPUS_Riometer_Baselining.pdf](http://www.aurora.phys.ucalgary.ca.northstar/rio/doc/CANOPUS_Riometer_Baselining.pdf)].

Figure 1.2.2 shows the location of the Finnish chain of riometers in the northern

hemisphere where precipitation may be recorded due to observed ELF/VLF chorus in the southern hemisphere at SANAE.

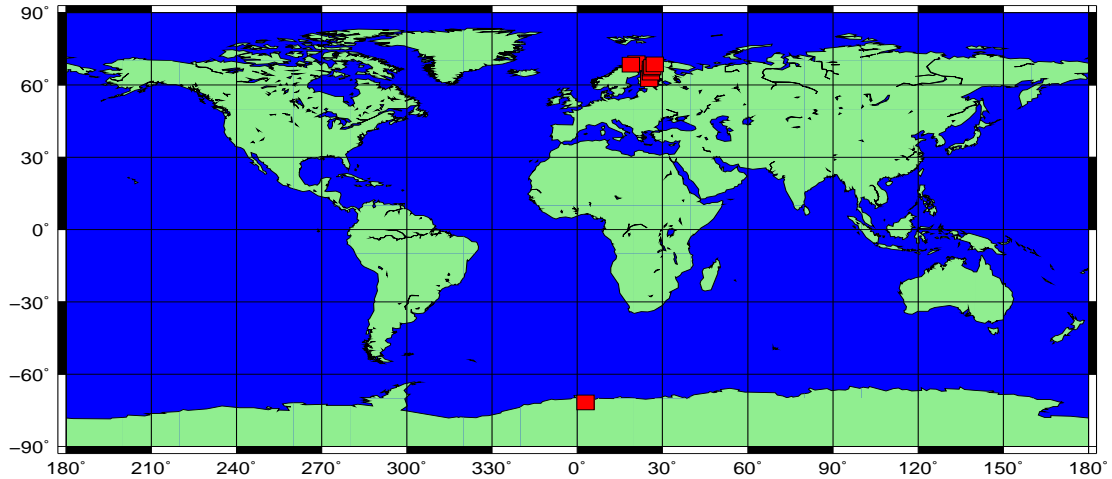


Figure 1.2.2: The location of SANAE and the Finnish chain of riometers(in red symbol)

Riometers are highly sensitive receivers which measure signals received from the sky [Nashimo et al., 1998]. Observations can be made with different orientations using an array of antenna elements.

Imaging riometers are used to determine the spatial distribution of enhanced ionisation. Precipitating particles cause an increase in the ionospheric electron density and also generate enhanced auroral excitation, which consequently cause augmented absorption of cosmic radio noise incident on the Earth [Wang et al., 1994]. The riometers in Finland are the *La Jolla* type, operating at three frequencies 30.0 MHz, 32.4 MHz and 51.4 MHz. However, to reduce any discrepancies due to different operating frequencies, we have used only measurements at 30.0 MHz and 32.4 MHz from the stations given in Table 1.2.1 on page 6.

FINNISH-RIO-ABS-CHAIN-STATIONS				
Station	Lat(N)	Lon(E)	Operating Frequency (MHz)	L - Value
Abisko	68.36°	18.82°	30.0	5.9
Ivalo	68.55°	27.28°	30.0	5.7
Sodankylä	67.42°	26.39°	30.0	5.3
Rovaniemi	66.78°	25.94°	32.4	5.1
Oulu	65.08°	25.90°	30.0	4.5
Jyväskylä	62.42°	25.28°	32.4	3.8

Table 1.2.1: Finnish chain of stations at different operating frequencies and L-values.

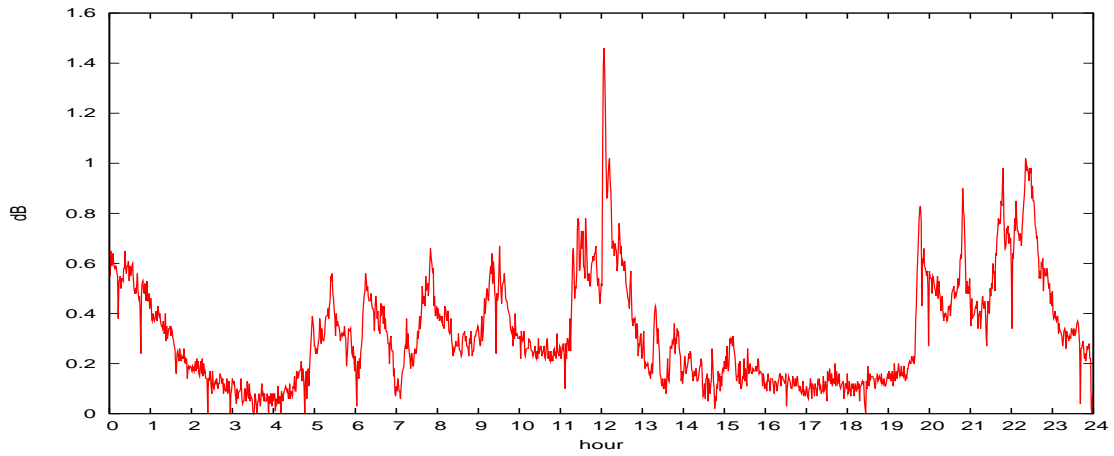


Figure 1.2.3: Riometer Absorption (dB) versus Time (UT) for Abisko

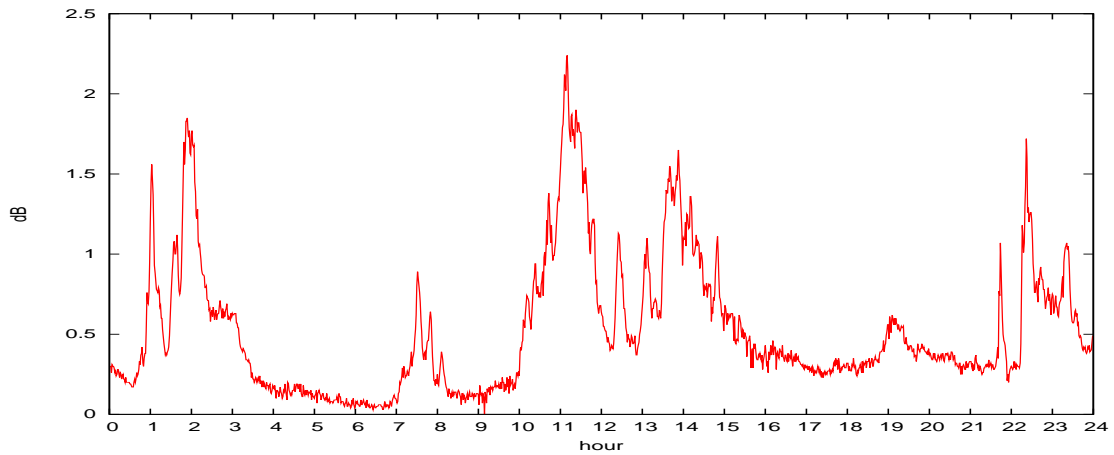


Figure 1.2.4: Riometer Absorption (dB) versus Time (UT) for Ivalo

Figures (1.2.4 and 1.2.5) are examples of ionospheric riometer absorption recorded at Abisko and Ivalo respectively. The peaks correspond to absorption in decibels(dB) which is given by the Equation 1.2.1 below.

$$Absorption(dB) = 10\log\frac{I}{I_o} \quad (1.2.1)$$

The two Figures (1.2.3 and 1.2.4) have a noticeable peak between 10 UT and noon which may be due to solar activity. The ionospheric density below 80 km is greatly influenced by the chemistry of the region on the sunward side of the earth where ionisation, particularly at lower altitudes, increases as a result of solar radiation [Ranta et al, 1984] which consequently increases ionospheric absorption. This daytime absorption is of no interest in our study as we use only night-time observations.

1.3 Outline

VLF and ELF chorus induced electron precipitation is what this thesis is concerned about, specifically by looking at changes in the ionisation levels in the D-region of the ionosphere recorded by riometers at a chain of stations in Finland, in the northern hemisphere, in relation to VLF chorus observations at SANAE, in the southern hemisphere. An overview of the magnetosphere and ionosphere are presented in the second chapter. In Chapter 3 various aspects of VLF waves in the magnetosphere are given, wave-particle interactions are discussed and the processes which produce chorus are outlined. Chapter 4 presents case studies in which chorus and its possible association with absorption are studied, and Chapter 5 presents and discusses VLF statistics. Chapter 6 introduces a new index of VLF activity which gives a measure of the level of VLF noise and also an indication of the nature of the signal. Chapter 7 is a discussion of the findings of chapters 4, 5 and 6.

Chapter 2

The Magnetosphere and Ionosphere

2.1 Introduction

The Solar-terrestrial environment, also known as geospace, is the domain of Sun-Earth interactions. It consists of particles, fields and radiation from the Sun to the Earth's space environment and upper atmosphere.

Geospace is considered to be the fourth physical geosphere after solid Earth, oceans, and atmosphere [http://stp.gsfc.nasa.gov/stp_dictionary.htm].

The regions of geospace that are important to this study are the magnetosphere and ionosphere and their properties are briefly summarised here.

2.2 Magnetosphere

The magnetosphere is a cavity created by the solar wind and the terrestrial magnetic field. Its sunward boundary 'magnetopause' is determined by the balance of the kinetic pressure of the solar wind and the magnetic pressure of the Earth's field.

For a solar wind with particle density n particles m^{-3} an average mass m and velocity v incident at an angle ψ to the normal at the boundary. The number of particles striking per unit area per unit time is $nv\cos\psi$. If specular reflection is assumed the rate of change of momentum is $2mnv^2\cos^2\psi$ per unit area. Balancing this against dipole field magnetic pressure yields the boundary as shown in the Equation (2.2.1) below.

$$2mnv^2\cos^2\psi = \frac{B^2}{2\mu_0} \quad (2.2.1)$$

But at the equator $\psi = 0$ and $B = \frac{B_o}{r^3}$ where B_o is the magnetic field on the Earth's surface at the equator, and thus Equation (2.2.1) becomes;

$$r^3 = \frac{0.5B_o}{v\sqrt{\mu_o nm}} \quad (2.2.2)$$

Equation (2.2.2) gives the equatorial 'stand-off' distance of the magnetospheric boundary in the sunward direction, and as can be seen, its position changes with changes in density and speed of the solar wind. This forward boundary, during quiet times, lies at about $10R_E$.

This is a region where the motion of charged particles is dominated by the Earth's magnetic field. It extends from the topside of the ionosphere to approximately $10R_E$ in the solar direction of the magnetopause on the sunward side of Earth. The structure of the magnetosphere is shown in Figure 2.2.1. The supersonic flow of the solar wind is distorted by the Earth's magnetic field forming a bow shock on the sunward side of the Earth where the flow is reduced, heated and diverted around the Earth. Like other shock waves, the bow shock of the magnetosphere represents a transition between supersonic and subsonic flow. Thus, inside the bow shock there is a region of subsonically flowing plasma. This region is called *magnetosheath*. Here the plasma density is higher than in the solar wind because the flow rate is reduced.

The magnetospheric cavity formed is due to the restricted Earth's magnetic field by the dynamic pressure of the solar wind and the cavity is bounded by the *magnetopause*. The magnetosphere is stretched on the anti-solar direction to form a tail consisting of the south and north lobes which are made up of tenuous plasma ($N \lesssim 0.1cm^{-3}$) and oppositely directed magnetic fields. The two lobes are separated by the plasma sheet which contains $\sim 1keV$ hot plasma. They are called south and north because they connect magnetically at the polar caps of the Earth. The magnetic field in the south lobe is directed away from the Earth whereas in the north lobe, it is directed towards the Earth [Hughes, W.J]. The configuration of the magnetotail can be considered to be due to a current sheet flowing from the dawn side to the dusk side across the 'neutral' sheet between the north and the south lobes of the tail. These currents 'close' around the surface of the tail.

Since, the dynamics of charged particles are principally determined by the magnetic field configurations, there are curvature and gradient drifts as a consequence. Electric fields due to the rotation of the Earth and the interaction of the Interplanetary Magnetic Field (IMF) with the Earth's magnetic field, also produce drift motions.

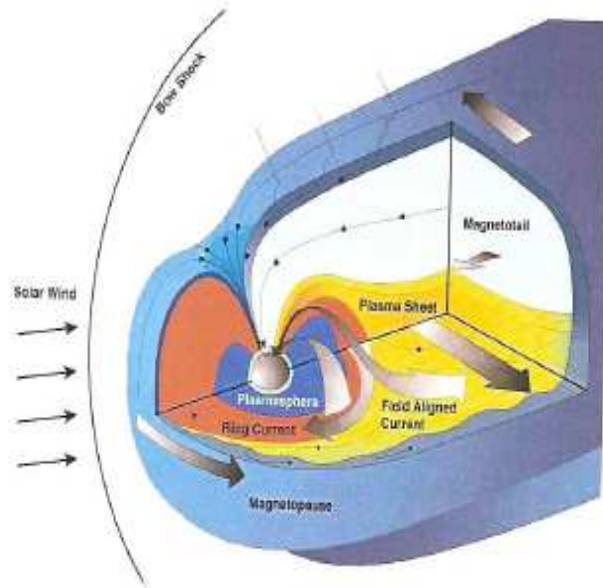


Figure 2.2.1: Schematic representation of the terrestrial magnetosphere.

The plasma drifts towards the current sheet through the lobes by “ $E \times B$ ” drift . These drifts divide the magnetospheric plasma into two different types, one of which co-rotates with the Earth, while the other type is convected sunward from the tail. Closest to the Earth, on magnetic field lines originating at low and middle geomagnetic latitudes, there is a comparatively dense plasma, which forms the *plasmasphere*. This plasma is a kind of continuation of the ionosphere underneath it and from which it is formed by diffusive transport from high density region. The temperature is essentially the same as in the ionosphere, i.e, some thousands of K, except in the outermost regions, the density decreases gradually from ionospheric densities to values of 10 - 100 particles per cubic centimeter. The outer boundary of the plasmasphere, the *plasmopause*, is a magnetic field-aligned density discontinuity that separates the plasmasphere, populated by cold ($\sim 1eV$) dense ($N \sim 10^3cm^{-3}$) plasma of predominantly ionospheric origin, from the plasmatrough, which contains a relatively sparse ($N \sim 1^3cm^{-3}$) plasma originating primarily in the solar wind [Carpenter, 1963, Gringauz, 1963].

The speed and density of the solar wind as well as the orientation of the IMF highly determines the form and processes taking place within the magnetosphere. Magnetic reconnection on the dayside magnetopause allows interplanetary and terrestrial magnetic field lines to merge. Magnetospheric plasma and solarwind can then interact along open field lines. The reconnection rate is regulated by the north-south component of the IMF, being most intense when the IMF is directed antiparallel to the Earth's magnetic field. Reconnected field lines are dragged across the Earth's magnetic poles by the motion of the solar wind and hang over the magnetotail. On average, the antisunward flow of open field lines is balanced by the sunward convection of closed field lines. There is continuous reconnection occurring within the magnetotail at a distant neutral line some $100 R_E$ down the tail.

The structure of the magnetosphere is incomplete without an account of the particles of higher energy, generally known as *the trapped radiation or the Van Allen particles*. The Van Allen radiation belts are regions of high-energy particles, mainly protons and electrons, held captive by the magnetic influence of the Earth. These particles comprise the diffuse and discrete auroral precipitation within the auroral zone, the energetic magnetospheric electrons extending from mid-latitudes throughout the auroral zone and the ring current particles precipitating at mid-latitudes.

2.2.1 Trapping of Particles

Charged particles in the solar wind flowing directly from the sun towards the Earth encounter the magnetosphere and thus do not readily travel across a magnetic field but are deflected around the magnetosphere. However, some solar wind particles moving along the Earth's magnetic field lines find themselves in the Van Allen radiation belts. The Earth is however the source of most of the particles in these belts. When air particles diffuse into space from the Earth they become ionised by solar radiation and are drifted by the Earth's magnetic field.

High-energy protons largely populate the inner belt, with a few million eV energies, as a result of cosmic rays knocking particles out of the upper atmosphere. On the other hand, the major constituent of the outer belt is populated mainly with high-energy electrons, with a few thousand eV energies, due to magnetospheric acceleration processes and cosmic rays. During steady state conditions in the magnetosphere, particles neither enter nor escape these trapped orbits. However the accelerated particles may enter and leave the Van Allen belts during magnetospheric disturbances and undergo

three kinds of motion due to the Earth's magnetic field.

1. Spiral motion in which protons and electrons gyrate around, and move along magnetic field lines.
2. Drift motion in which particles drift around the earth relatively slowly. Protons drift westwards whilst electrons drift eastwards. This motion takes place on magnetic shells characterised by the constant values of the McIlwain parameter L [Redhill, 1976]. The drift motion arises due to the gradients and curvature of the magnetic field
3. The bounce motion where particles bounce back and forth from one hemisphere of the Earth to the other as they spiral around the field lines of the Earth's magnetic field. The reflection or mirroring of particles is caused by the convergence of magnetic field lines near the poles (mirror points).

2.3 Ionosphere

The Sun's radiation on the Earth's upper atmosphere has an ionising action which produces free electrons. Above 60 km, the number of these free electrons is sufficient to affect the propagation of radio waves. This ionised region of the atmosphere is a plasma, known as the *ionosphere* and extends from 50 km to several Earth radii [Davies, 1990]. The ionosphere is coupled to both the magnetosphere and the neutral atmosphere and has three major sections, lower ionosphere (50 - 90 km), bottomside ionosphere (90 - \sim 350 km) and the topside ionosphere which extends beyond 350 km. The peak electron density falls in the F region (150 km and above), [Davies, 1990].

Because of the difference in ionisation density at various ionospheric levels, there are various layers in the ionosphere referred to as the D-, E- and F-regions that interact with radio waves differently. Their location is shown in Figure (2.3.1). The regions are important for "High Frequency (HF)" propagation studies as they refract HF waves. Electromagnetic radiation from the Sun is the major source of ionisation [Baker, 2004].

The F-region, which lies within the altitude range of about 150 km to about 400 km, is ionised by Ultra Violet(100 - 100Å) radiation from the Sun. This region varies with time e.g. during the day it is made up of F1 and F2 regions which combine at night to form the F-region. This region is responsible for refracting HF radio waves (10 - 15 MHz).

Much higher frequencies in the F-region are reflected than in the region below it, and the highest frequency reflected by this region is known as the Maximum Usable Frequency (MUF).

The E-region extends from 90 km to 150 km and is ionised only during the day by soft X-rays with wavelengths in the range (10 - 100Å). The rate of photoionisation and recombination in the E-region is slower than that in the D-region [McNamara, 1991].

The D-region lies between about 50 km and 90 km and is the closest ionospheric layer to the Earth's surface. However it disappears at night making the atmosphere more accessible to VLF and LF waves. This region absorbs frequencies below 10 MHz and allows higher frequencies to penetrate to outer layers and is ionised by hard X-ray radiation from the Sun at wavelengths 1 to 10Å.

Understanding the ionosphere is very important, for example in telecommunication longer wavelength radio signals propagate through the Earth-ionosphere wave guide allowing radio communication over the horizon. This is how the long, medium and short wave radio broadcasts reach receivers over long distances. As the ionosphere is not a smooth reflector for electromagnetic radio waves, the signal can be scattered in many directions causing loss of signal strength and interference from other transmitters.

Particles injected in magnetic sub-storms disturb the ionosphere particularly in the auroral regions.

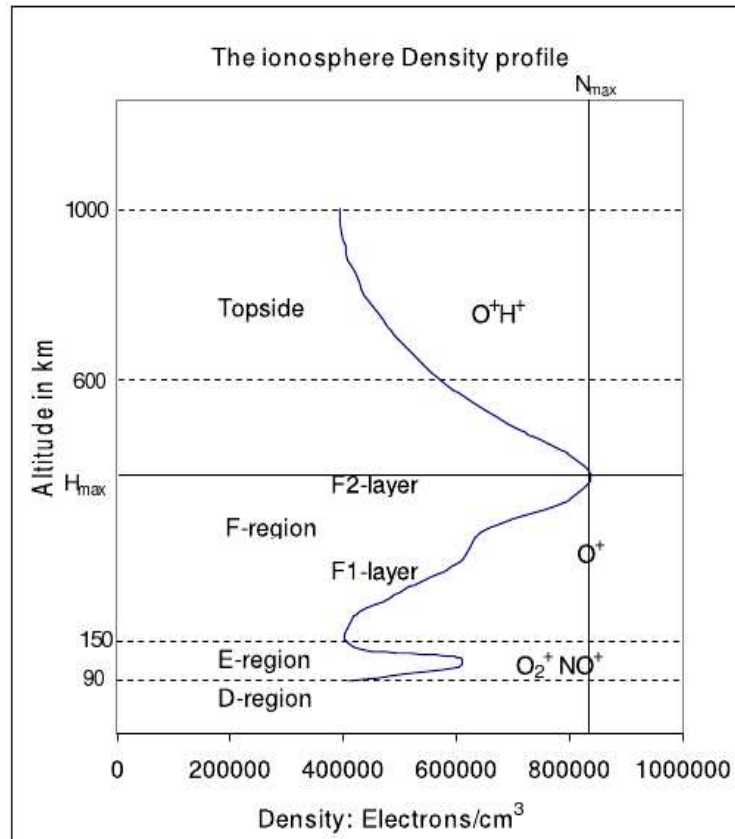


Figure 2.3.1: A typical electron density altitude profile, the most important ions, and various ionospheric layers. From http://www.dcs.lancs.ac.uk/iono/ionosphere_intro/

High energy particles emitted from the Sun and in the cosmic background contribute to the ionisation levels of the ionosphere alongside solar radiation induced ionisation. The amount of ionisation produced in this way is generally much less than that produced by electromagnetic radiation. Moreover, at night when there is very little or no solar illumination, there are minimal ionisation levels due to the precipitation of electrons induced by wave-particle interaction in the magnetosphere. If the precipitation is sufficiently intense, enhanced absorption may be recorded by suitably located riometers and this is investigated in this thesis. For further reading on the ionosphere, the reader is referred to [Davies, 1990 and McNamara, 1991].

2.4 Collision Frequency versus Altitude

The variation of the collision frequency relative to altitude is shown in Figure 2.4.1, the collision frequency is one of the major factors that determine ionospheric absorption and this varies with altitude. At high altitudes the density of ions and electrons and other molecules is considerably low and consequently the collision frequency is low. As a result, the attenuation of radio waves at high altitudes is minimal for a significant ionospheric absorption to be observed.

Most of the attenuation occurs at lower altitude in the D layer, because the density of neutral atmosphere is high and thus the number of electron collisions is high. When a signal enters the D region, it transfers energy to the electrons and sets them in motion, vibrating in phase with the radio signal. As electrons vibrate in this manner, they can collide with other molecules, ions, or electrons and every time this happens, a small amount of energy is dissipated, and this is manifested as a loss in the strength of the signal. The overall amount of signal attenuation is highest at lower altitude because of increased collision frequency.

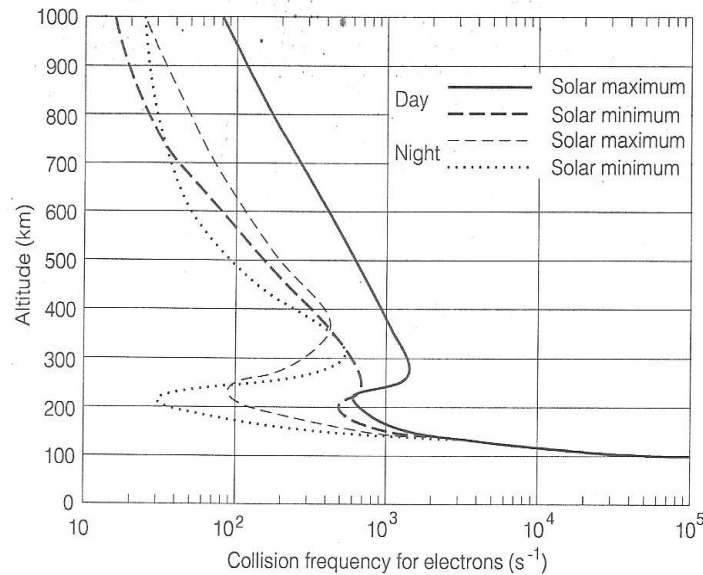


Figure 2.4.1: Altitude variation vs collision frequency of electrons [Hanson, 1965]

Chapter 3

VLF Waves

3.1 Introduction

The acronym VLF stands for Very Low Frequency and defines the electromagnetic frequency band that extends from 3 kHz to 30 kHz. In practice we will be concerned only with the lower end of its band, <5 kHz. The only significant form of electromagnetic radiation within the terrestrial magnetosphere in the VLF range is that which propagates in the whistler mode and these can penetrate the ionosphere and be received on the ground. These waves may emanate from a variety of sources. On Earth they are produced either naturally by lightning discharges or artificially by power line harmonic radiation, navigation and military transmitters, while in space they can be generated by wave-particle interactions.

3.2 The Whistler Mode

The propagation of electro-magnetic waves with frequencies significantly higher than the ion gyrofrequencies through cold homogeneous plasma is described by the Appleton-Hartree equation [Helliwell, 1965]. The meaning of the symbols used in the equations may be found in the nomenclature table on page (iv).

$$n^2 = 1 - \frac{X}{1 - \frac{Y^2 \sin^2 \theta \pm \sqrt{Y^4 \sin^4 \theta + 4Y^2 \cos^2 \theta (1-X)^2}}{2(1-X)}}} \quad (3.2.1)$$

The equation above has the collision frequency neglected, θ is the angle between the wave normal vector and the static magnetic field, $X = \frac{\omega_p^2}{\omega^2}$ and $Y = \frac{\Omega}{\omega} = \frac{1}{\Lambda}$, and heavy

ions are assumed not to affect the propagation.

By considering quasi-longitudinal propagation (whistler mode) we can neglect constants transverse to B_o direction. In this Equation (3.2.1) reduces to:

$$n^2 = \frac{\omega_p^2}{\omega(\Omega \cos\theta - \omega)} \quad (3.2.2)$$

Equation (3.2.2) is the whistler or quasi-longitudinal (QL) approximation [Helliwell, 1965]. In the magnetosphere the QL approximation holds for an appreciable range of θ . Thus the refractive index depends not only on the frequency but also on the direction of propagation, consequently whistler mode waves are dispersive and anisotropic.

This expression enables us to calculate the phase and group velocities of the wave, v_p and v_g by:

$$v_p = \frac{\omega}{k} = \frac{c}{n} \text{ and } v_g = \frac{d\omega}{dk}$$

Note that the group velocity $\frac{d\omega}{dk}$ calculated in the conventional way is the velocity parallel to the wave normal and differs from V_R the ray velocity. This property is discussed in detail by Helliwell (1967, Ch 3).

The Equation (3.2.2) is undefined when the denominator is zero, this occurs when:

$$\cos\theta = \frac{\omega}{\Omega} \quad (3.2.3)$$

This defines a resonance cone, for the wave normal, about the magnetic field direction. The satisfaction of (3.2.3) yields electrostatic waves [Walker, 1993]. The effects of positive ions become significant at frequencies less than the lower hybrid resonance, where the resonance cone disappears [Walker, 1993]. The whistler mode applies only to frequencies less than the electron gyrofrequencies.

The whistler mode wave is loosely guided by the static magnetic field. An interesting feature of whistler mode propagation is that the direction of energy propagation (ray direction) is not parallel to the wave normal, a fact which leads to the loose guiding of the wave by the magnetic field illustrated in Figure 3.2.1, which gives the ray direction, β , with respect to the wave normal angle for a range of normalised frequencies.

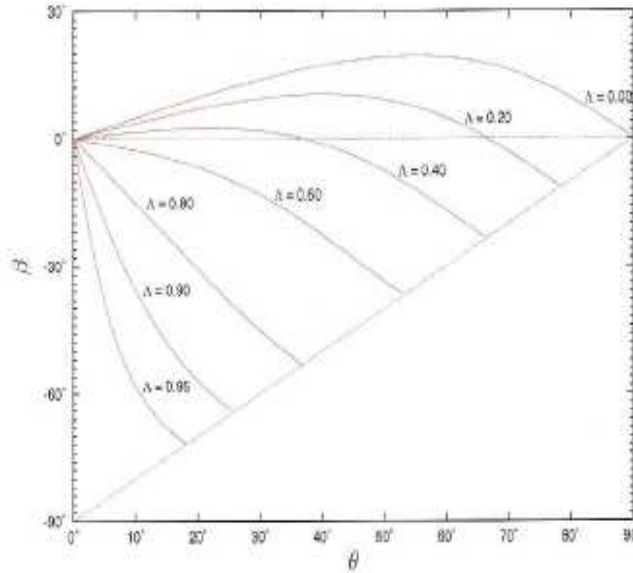


Figure 3.2.1: beta as a function of wave normal angle, theta. Collier [2006, Figure 3-1].

The speed of propagation at a given frequency does not change appreciably with angle to the static magnetic field for moderate values of Λ , and the wave energy moves in the direction of the magnetic field. The guiding effect of the magnetic field is lost as Λ goes to 1.

Whistler mode energy may propagate in field aligned ducts of enhanced plasma for $\omega < \frac{\omega_H}{2}$. This couples the propagation to the magnetic field direction. Whistler mode energy may also propagate in ducts of depleted plasma density for $\omega > \frac{\omega_H}{2}$.

VLF waves propagate in the earth-ionosphere waveguide and under certain circumstances may enter into the ionosphere and magnetosphere.

The coupling of VLF waves across the refractive index boundary between the earth-ionosphere waveguide and a duct in the ionosphere is illustrated in Figure 3.2.2. The refractive index surface is spherical in the neutral atmosphere, however in the ionised upper atmosphere it is a surface of revolution around the magnetic field direction. The mapping of the wave normal vector from the atmosphere into the ionosphere is determined by Snell's law and this consequently defines a range of angles referred to as the transmission cone. In conditions where the transmission and trapping cones overlap we get coupling from the waveguide to a duct in the magnetosphere. The opening angles of the two cones and inclination of the magnetic field determines the degree of overlap. The efficiency of coupling is high when the magnetic field is normal to the ionosphere. Waves which are incident from higher latitudes experience more effective coupling for an oblique magnetic field [Helliwell, 1965, Figure 3-23].

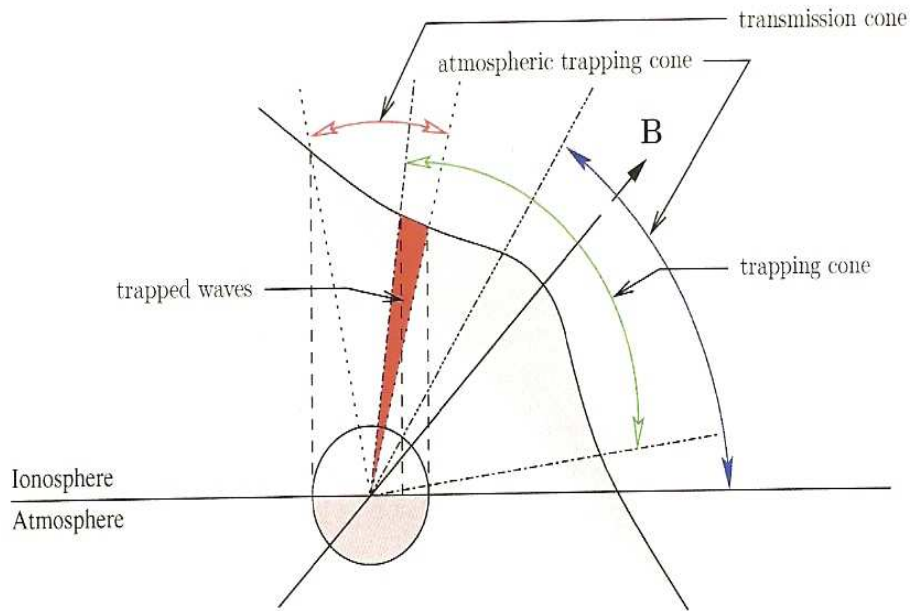


Figure 3.2.2: The coupling of VLF waves from the atmosphere to the ionosphere. Collier (2006)

3.3 Wave-Particle Interaction

3.3.1 Introduction

Wave-particle interactions play important roles in many phenomena taking place in the laboratory [Gill, 1981] and in space plasmas [Gary, 1992]. Here we are concerned only with wave-particle interactions in space plasmas. However, in laboratory plasmas, wave-particle interactions have many important applications, such as plasma heating by radio waves at ion and electron cyclotron frequencies, beat wave acceleration and transport losses due to edge turbulence whereas in space plasmas, wave-particle interactions are thought to be important for the formation of the magnetopause boundary layer, generation of electromagnetic outer zone chorus and plasmaspheric hiss emissions, and the precipitation of particles causing aurorae [Tsurutani and Lakhina, 1997].

In the magnetosphere, low-frequency waves can interact with charged particles over long spatial scale lengths and this is thought to be a conveyor of energy from one region to another. Here pitch angle scattering as a result of cyclotron resonance between outer zone whistler mode chorus and 10 keV to 100 keV trapped substorm electrons can lead to electron precipitation [Tsurutani and Lakhina, 1997]. These precipitating electrons produce various ionospheric phenomena such as diffuse aurorae, enhanced ionisation in the ionospheric D and E regions and X ray bremsstrahlung.

3.3.2 Dynamics of Energetic Charged Particles

For a moving charged particle with charge q and velocity \vec{v} in a magnetic field \vec{B} , experiences a force

$$\vec{F} = q\vec{v} \times \vec{B} \quad (3.3.2.1)$$

It can be seen from Equation (3.3.2.1) that the force is orthogonal to both the velocity \vec{v} and the magnetic field \vec{B} . Consequently, the particles will generally move in a spiral motion along the magnetic field thus affecting the mobility of electrons and protons differently, i.e they gyrate in opposite directions.

The particle will only move in a straight line if the velocity \vec{v} , is purely parallel to the magnetic field \vec{B} in which case the force is zero. However, when the velocity is purely perpendicular to \vec{B} , the particle moves in a circle. The particle velocity can be divided into two components, V_{\perp} perpendicular to \vec{B} and V_{\parallel} parallel to \vec{B} . The

pitch angle is the angle between the velocity vector and the magnetic field direction and is given by $\tan \alpha = \frac{v_{\perp}}{v_{\parallel}}$. Thus, we can rewrite Equation (3.2.2.1) in scalar form as $F = ev_{\perp}B = ev \sin \alpha B$. The gyroradius can be obtained from the centripetal force on a particle with mass m , $\frac{mv_{\perp}^2}{r_B} = \frac{mv^2 \sin^2 \alpha}{r_B}$, giving a gyroradius of:

$$r_B = \frac{mv \sin \alpha}{qB} \quad (3.3.2.2)$$

The angular electron gyrofrequency (Ω_e) is given by $\tau = \frac{2\pi}{\Omega_e} = \frac{2\pi r_B}{v \sin \alpha} = \frac{2\pi m}{qB}$, and may be written:

$$\Omega_e = \frac{qB}{m} \quad (3.3.2.3)$$

If there is no significant change in the magnetic field during one gyroradius, no work is done on the particle and its energy remains constant, thus

$$\Phi_m = \pi r_B^2 B = \frac{2\pi m^2 v^2 \sin^2 \alpha}{q^2 B} = Const \quad (3.3.2.4)$$

this reduces to:

$$\frac{\sin^2 \alpha}{B} = Const \quad (3.3.2.5)$$

(assuming v^2 is constant).

Equation (3.3.2.5) gives the pitch angle of the particle in the earth's magnetic field along the particle trajectory.

$$\frac{\sin^2 \alpha}{B} = \frac{\sin^2 \alpha_{eq}}{B_{eq}} = \frac{1}{B_m} \quad (3.3.2.6)$$

The pitch angle will always increase as the particle moves away from the equatorial plane since $B_{eq} < B$ and equal 90° at B_m , the particle mirror point. If B_m is at an altitude where the collision frequency is high the particle will collide with neutral atmospheric particles and will precipitate into the earth's atmosphere. We thus define *loss cone pitch angle* (α_{lc}), which is the equatorial pitch angle above which all particles will mirror and below which all particles will precipitate. This can be seen in Figure (3.3.2.1) as a cone about the magnetic field direction.

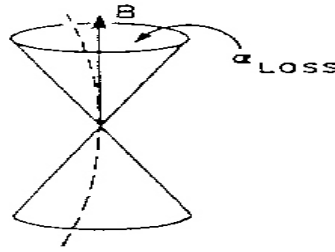


Figure 3.3.2.1: Diagram illustrating the loss cone. From Roederer [1970]

3.3.3 Doppler-Shifted Cyclotron Resonance

In the magnetosphere, there are a number of possible wave-particle resonances, however we are concerned only with Doppler-shifted cyclotron resonance involving right-hand circularly polarised whistler-mode waves and radiation belt electrons (transverse resonance), refer to Figure 3.3.3.1.

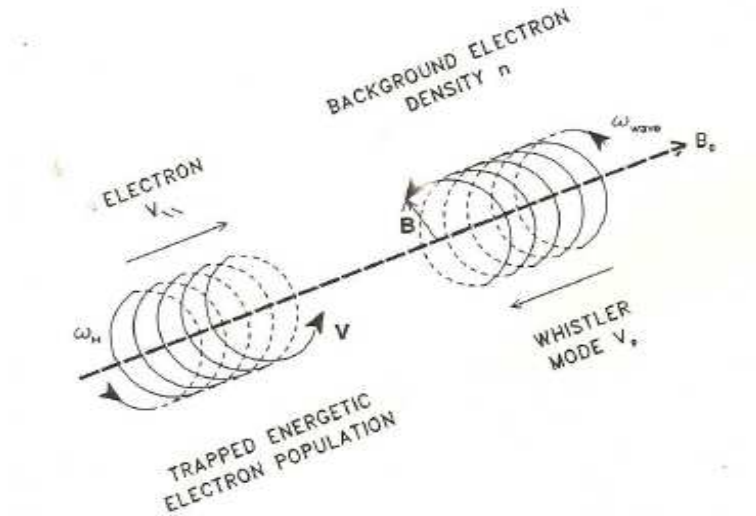


Figure 3.3.3.1: For effective interaction the electric vector of the whistler must be maintained parallel to the velocity of the electron. Hargreaves [1979, Figure 9-2]

It is known as transverse resonance because it involves the particle's perpendicular velocity component to the geomagnetic field.

It is known that the electrons gyrate with f_B whereas whistler-mode wave frequencies fall anywhere between $f < f_B$. For resonance to be achieved, the wave frequency and the electron gyrofrequency should be matched. If this condition is met there can, under certain conditions, be a transfer of energy between the waves and electrons. At resonance, the wave frequency is Doppler-shifted to match the gyrofrequency of the counter-streaming electrons and hence the name Doppler-shifted cyclotron resonance. It should be noted that, for an efficient energy transfer the particle and the wave must maintain a sufficient phase relation.

The condition for the fundamental resonance is expressed by

$$\Omega_e = \omega - k \cdot v_{\parallel} \quad (3.3.3.1)$$

From Equation (3.3.3.1), it can be seen that particles with larger v_{\parallel} will resonate with lower wave frequencies. If the electron velocity is close to the speed of light Ω_e must be divided by γ , the relativistic correction. Because \vec{k} is along \vec{B} , the resonance condition is seen to depend on the electrons' parallel velocity v_{\parallel} as shown in Equation (3.3.3.1). If the pitch angle is known, the electron's total velocity and hence energy can be determined. Electrons may undergo pitch angle diffusion during the interaction [Kennel and Petscheck, 1966] with some electrons diffusing into the loss cone and precipitating into the upper atmosphere. The diffusion of electrons is along surfaces in velocity space defined by the resonance condition [Lyons and Williams, 1984]. An increase in electron energy causes wave damping while a decrease in the electron energy causes wave growth and this depends on the form of the electron distribution function. The most likely distribution in this case is the loss cone distribution, which results in cyclotron wave growth as the electrons diffuse into the loss cone [Lyons and Williams, 1984]. The area near the equatorial plane is the optimal region for the cyclotron resonance interaction because this is where the magnetic field changes the slowest and hence the resonance condition is satisfied for the longest period. Liemohn [1967], showed that the optimum region may be a few degrees away from the equatorial plane due to enhanced pitch angle anisotropy.

3.4 Types of Emissions Observed

In science there are discoveries which are accidental, among the many, whistlers and the related phenomena are just but some. They comprise a group of complex and fascinating

natural events that can be heard on a very low frequency equipment [Helliwell,1965].

3.4.1 VLF Whistler

A Whistler is a descending VLF tone, produced by waves from terrestrial lightning after propagation through the magnetosphere [Storey, 1953; Helliwell, 1965]. Lightning is a fleeting source of electromagnetic radiation, producing a broad-band pulse which propagates through the atmosphere in the Earth-ionosphere wave-guide. All frequencies travel at the same rate in the atmosphere and are detected as atmospherics or in short spheric. However, some fraction of the energy may penetrate through the ionosphere into the magnetosphere. Here these waves are likely to couple to a duct and consequently be guided to the conjugate hemisphere, where a part of the incident radiation penetrates through to the ground. The characteristic frequency-time structure of a whistler is as a result of the dispersive passage of the pulse through the magnetospheric plasma which causes a frequency-dependent delay. Whistlers may be used as passive space probes as they travel many earth radii beyond the Earth's surface providing information about the distribution of ionization in the outer atmosphere [Helliwell, 1965]. Their analysis has led to a deeper understanding of the near-Earth space environment [e.g.,Carpenter, 1963]

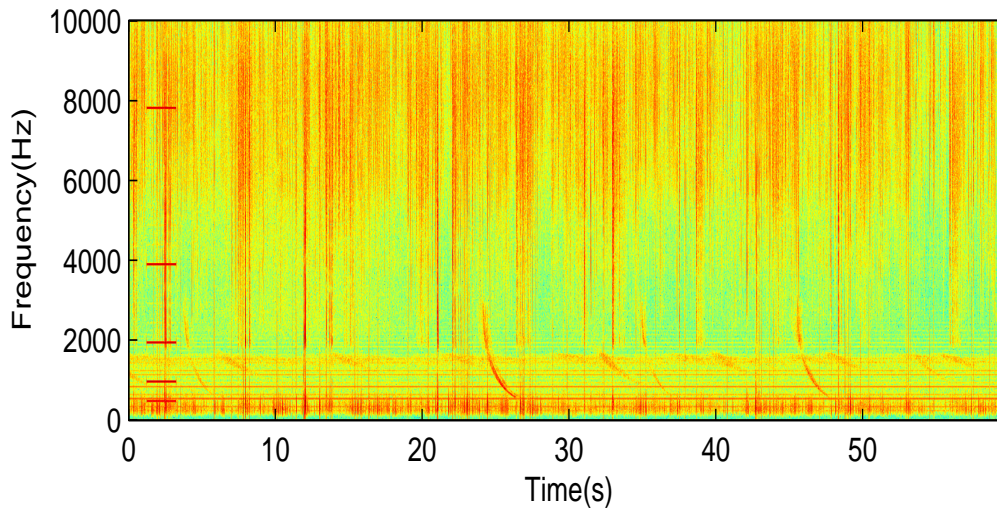


Figure 3.4.1.1: Spectrogram of whistlers recorded at SANAE

The spectrogram in Figure 3.4.1.1 shows an example of whistlers recorded at SANAE on day 275 of 2005 at 0030UT. Whistlers are seen at ~ 25 s and ~ 47 s in the figure.

3.4.2 VLF Chorus

Chorus is a VLF and ELF electromagnetic radio signature commonly observed both in the magnetosphere and on the ground. It usually consists of numerous brief discrete rising tones (refer to Figure 5.2.2), and sounds like the chatting of birds. Here the signature has typical periods from 0.1s to a maximum of 0.2s and the spectral structure is mainly composed of rising tones. Chorus is often accompanied by other spectral shapes such as constant tones, inverted and non inverted hooks.

A phenomenological theory was put forward by Helliwell based on cyclotron resonance, to explain generation of of variable - frequency discrete VLF emission. Energetic electrons are phase-correlated by circularly polarised waves in the whistler mode within the interaction region and then radiate. The lowering of their mirror altitudes is as a result of energy loss of the interacting electrons, as shown by *Brice* [1964a, b]. Since the resonance condition requires that Doppler-shifted wave frequency be matched to the electron gyrofrequency, the cyclotron radiation and resonant electrons travel in opposite directions along the field line [Helliwell, Katsufraks and Rosenberg, 1971]. The frequency-time characteristic of the emitted radiation depends on the position of the interaction region with respect to the equator. Falling tones are thus produced when the interaction region is on the upstream side (i.e., electrons moving in the direction of decreasing gyrofrequency) whereas the rising tones are produced when the interaction region is on the downstream side (i.e., electrons moving in the direction of increasing gyrofrequency) [Helliwell, Katsufraks and Rosenberg, 1971] and the constant frequency tones are generated on the equator.

Chorus is generated near the equatorial region by the transfer of energy from the radiation belt electrons to the whistler mode waves by the cyclotron resonance interaction [S.S Sazhin and M.Hayakawa, 1992]. Another mechanism has been proposed by Trakhtengerts (1999) for the generation of chorus which is based on the backward wave oscillator (BWO) regime of the magnetospheric cyclotron maser [Trakhtengerts, 1999; Kozelov and Tivota, 2002].

Chorus here is associated with magnetospheric substorms and particle injections [Isenberg et al, 1982] as is evidenced by the fact that its frequency of observation varies with time of day [Tsurutani and Smith, 1974, 1977].

Chorus at SANA E exhibits a $\frac{\Omega_{eq}}{2}$ cut-off which is likely to be related to propagation in a duct of enhanced plasma density for ground observations.

Chapter 4

Chorus and Absorption

4.1 Introduction

Precipitation of energetic charged particles into the ionosphere can be caused by a number of processes in interplanetary space and in the magnetosphere. We deal here only with electron precipitation induced by VLF waves in Doppler-shifted cyclotron resonance with counter-streaming electrons. Because the electrons are counter-streaming, the lower the velocity of the electrons the higher the frequency of the wave with which it is resonant.

Waves in cyclotron resonance with electrons can scatter electrons into the loss cone and produce electron precipitation. This occurs in anisotropic pitch angle electron distributions in which $T_{\perp} > T_{\parallel}$, where T_{\perp} and T_{\parallel} are the perpendicular and parallel energies. Such precipitation, if sufficiently intense, may lead to measurable absorption events. The question we are considering is whether such absorption events can be produced by chorus emissions. With this in mind we have selected chorus events recorded at SANAE and looked for absorption events recorded by the Finnish riometers.

A problem with the study is that the Finnish riometer chain is about 60°E in magnetic and geographic longitude of SANAE's conjugate point. As a consequence the local and magnetic local times at the Finnish stations will be later by about 4 hours from that of SANAE, for a given event.

Using the corrected geomagnetic coordinates model, we show the difference in local and magnetic local time using SANAE's conjugate point [$57.32^{\circ}316.87^{\circ}$] from that of the Finnish chain of stations using the difference in the geographic and geomagnetic longitude. The time difference is then computed on the basis that 15° in longitude is

equivalent to 1 hour in time. The time differences are calculated in Table 4.1.1.

The differences in MLT between SANAE and stations in the Finnish riometer chain mean that SANAE and the Finnish stations are observing events on field lines that link with different regions of the magnetosphere. Because of this we examine the data in two ways. In method 1, we make the assumption that when we observe chorus at a given MLT at SANAE, that on the same day similar conditions prevailed at the same MLT on the field lines that intersect the Finnish stations, in other words approximately 4 hours earlier in UT. In method 2 we look at events at all stations at the same UT. In this method if correlation is found between absorption events at one or more of the Finnish stations and chorus at SANAE it implies that the generation region for chorus extended sufficiently far in longitude to overlap the field line through the observing Finnish stations.

STATION——CONJUGATE										
	LAT	LON	MLAT	MLON	LAT	LON	MLAT	MLON	LT	MLT
Sanae	-71.67	357.17	-61.41	43.88	57.32	316.87	61.36	43.83		
Abisko	68.36	18.82	65.38	101.49	-60.37	61.93	-65.38	101.49	4 08	3 52
Ivalo	68.55	27.28	65.18	108.34	-58.63	66.63	-65.18	108.34	4 42	4 19
Sodankylä	67.42	26.39	64.07	106.89	-57.86	64.16	-64.07	106.89	4 38	4 12
Rovaniemi	66.78	25.94	63.43	106.14	-57.39	62.80	-63.43	106.14	4 36	4 09
Oulu	65.08	25.90	61.69	105.15	-55.84	59.90	-61.69	105.15	4 36	4 05
Jyväskylä	62.42	25.28	58.96	103.36	-53.33	55.23	-58.96	103.36	4 34	3 58

Table 4.1.1: Difference in LT and MLT from SANAE's CP for each riometer station

The two methods can be understood by referring to Figure 4.1.1. This is a schematic diagram showing SANAE where the chorus is recorded, and the Finnish chain where enhanced absorption is investigated.

In method 1 we look at chorus and absorption at the same MLT on the same day and in method 2 we use observations made at the same UT.

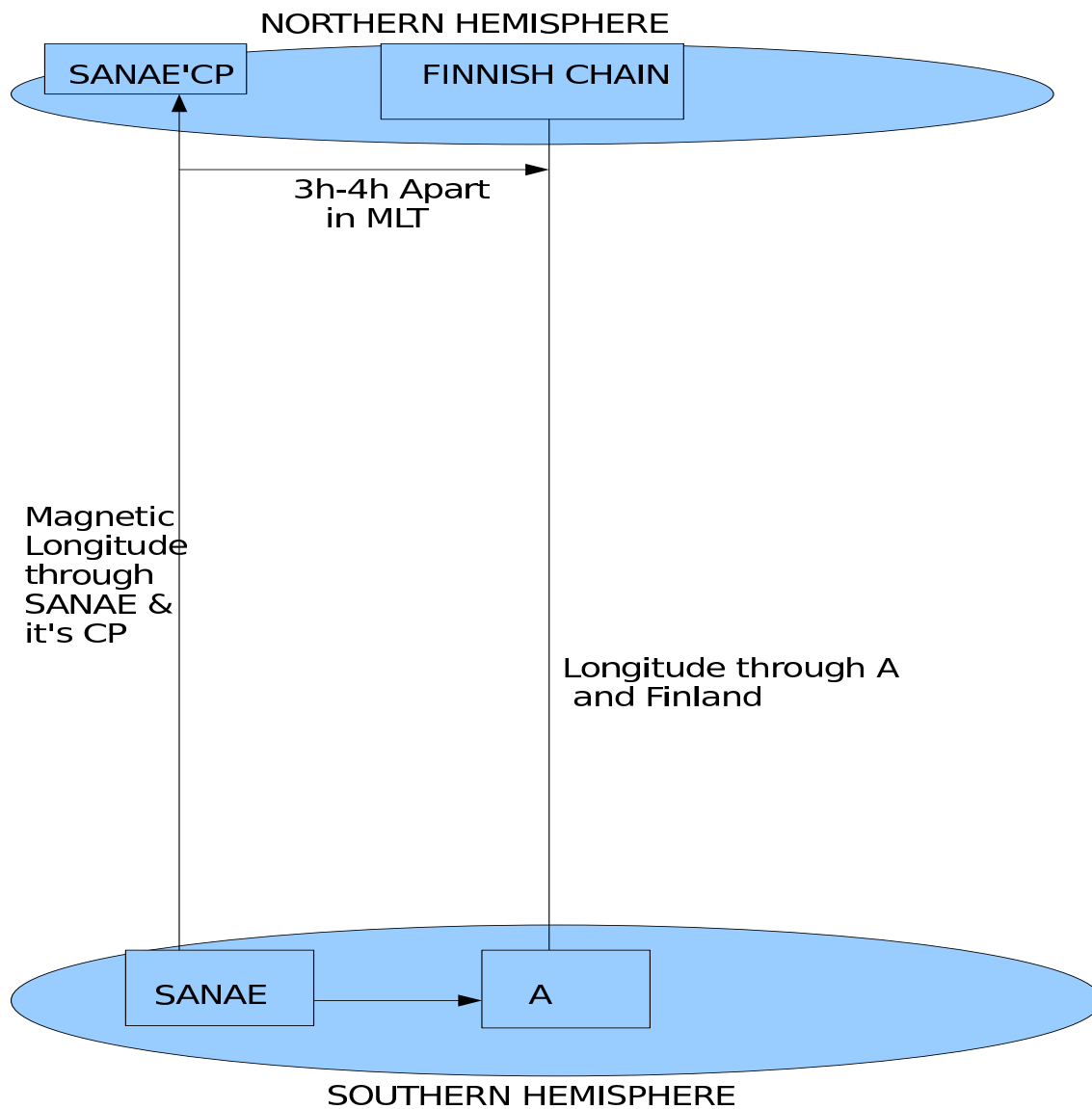


Figure 4.1.1: Chorus at SANA E & its relation to ionospheric absorption Finland

4.2 Case studies

Chorus events recorded at SANAE were studied to see if they corresponded to enhanced absorption events at the Finnish chain of riometers from $L = 3.8$ to $L = 5.9$ in the northern hemisphere.

In this section, studies on how VLF chorus is related to absorption observed on riometers are presented based on the assumption that the observed ionospheric absorption 4h earlier (first method) and at the same universal time (second method) when VLF chorus is recorded in the conjugate hemisphere is due to chorus induced precipitation.

We only look at absorption events that occur when the ionosphere over the Finnish stations is in darkness. This is to avoid confusion with absorption caused directly by solar emissions. The valid observing times are given in Figure 4.2.1.

Figure 4.2.1 shows an annual location of sunrise, sunset, dawn and dusk times for Finland with ‘Month Number’ on the horizontal axis and ‘Time(h)’ on the vertical axis. These are marked 1 and 2 respectively, whereas 4 represents ‘Darkness’ (in grey) and 5 represents ‘Dawn’ (in blue).

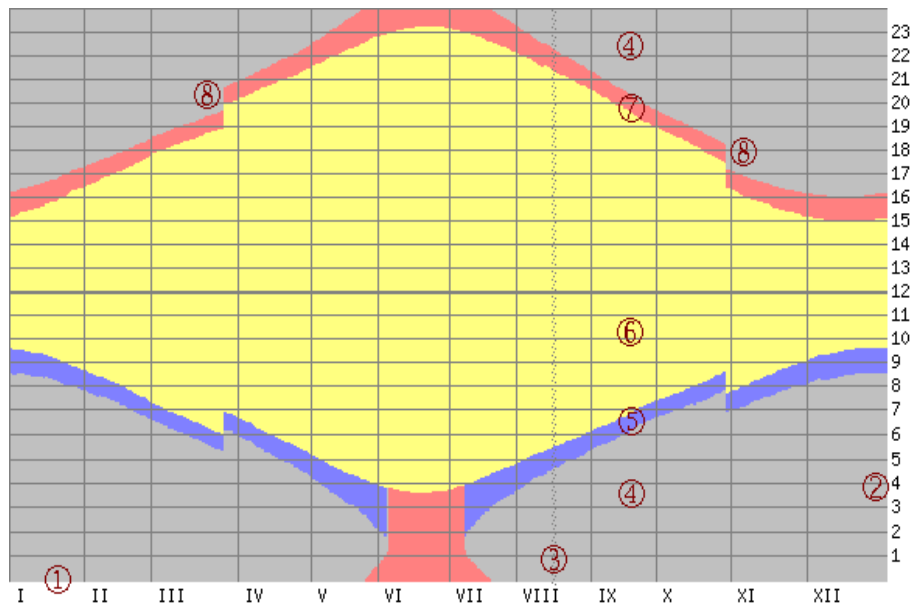


Figure 4.2.1: Solar graph: Month Number versus Time(LT) [<http://www.gaisma.com>]

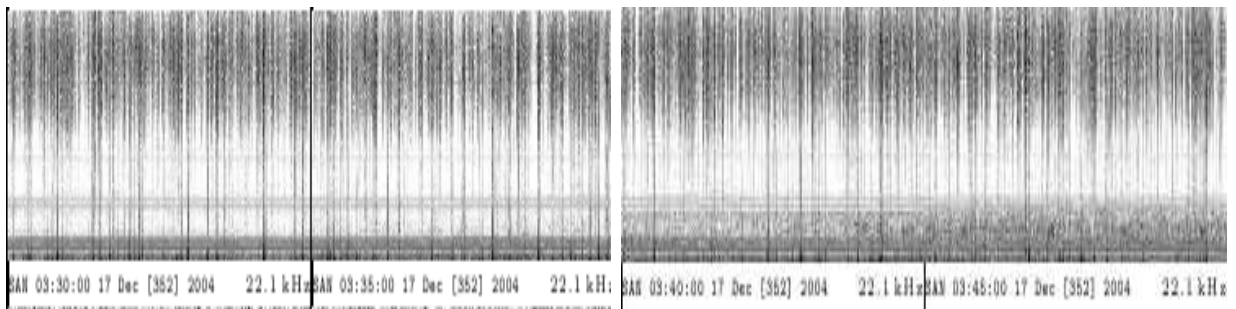
‘Sunshine’ (in yellow) is marked 6 and ‘Dusk’(in orange) is marked 7. We may read the day marked (3) in August for example as: dawn begins at $\sim 04:43$, the sun rises at $\sim 05:37$ and sets at $\sim 21:20$. Immediately dusk ends at $\sim 22:14$, darkness begins. The discontinuity in March and October, marked 8, is produced by the fact that the Finnish

operators use local time which in summer is corrected to Summer Time by advancing their clocks by one hour. Using Figure 4.2.1, we have selected chorus events at SANAE for times when the Finnish chain is in darkness.

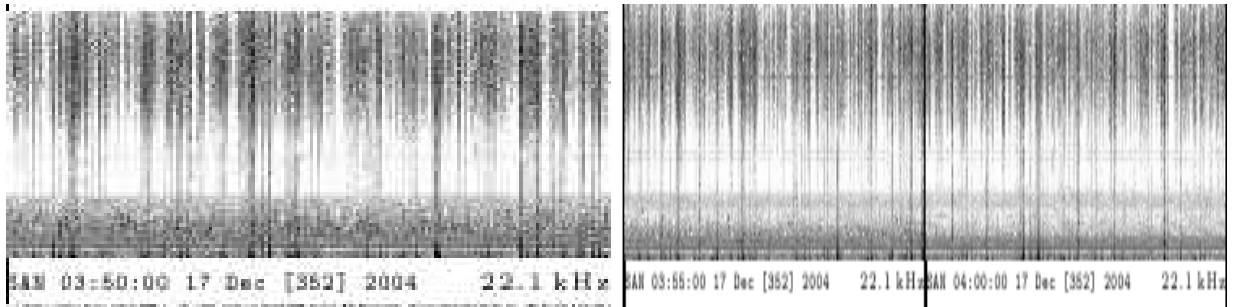
In the case studies we have used VLF data for 2004 and 2005 because chorus was more prevalent in these years. Limiting absorption measurements at the Finnish chain to the period from dawn to dusk, we discuss the observation in terms of two methods of absorption.

In diagrams e.g. Figure 4.2.4, to distinguish between the two methods of absorption, we have used letters A and B. The line associated with the letter A indicates when chorus would have occurred on the field lines through the Finnish stations if its pattern of occurrence in MLT was the same as that at SANAE. Letter B indicates when the chorus was actually observed at SANAE.

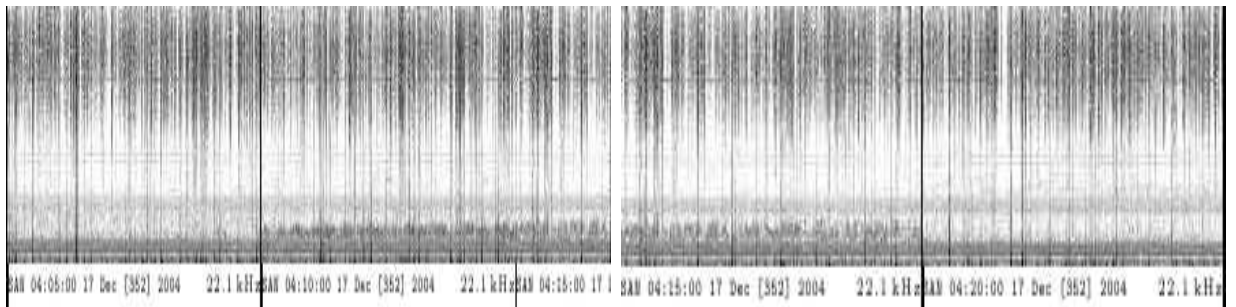
Figures 4.2.2 and 4.2.3 show VLF quicklooks from 0330 UT to 0440 UT and from 0445 UT to 0600 UT respectively, and were recorded on day 352 of 2004. Chorus is present between 0335 UT and 0600 UT with a changing upper boundary frequency between 1 kHz and 2 kHz; its intensity also varied with time. The vertical lines seen on the spectrograms are sferics. The spectrograms represent data recorded every 1 minute in 5 with frequency on the vertical scale from 0 to 10 kHz.



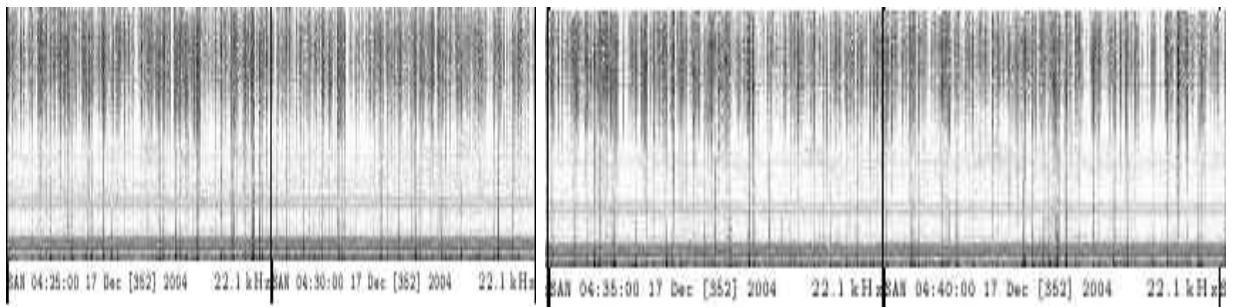
(a) VLF quicklook from 0330-0335UT of 17/12/04 (b) VLF quicklook from 0340-0345UT of 17/12/04



(c) VLF quicklook at 0350UT of 17/12/04 (d) VLF quicklook from 0355-0400UT of 17/12/04

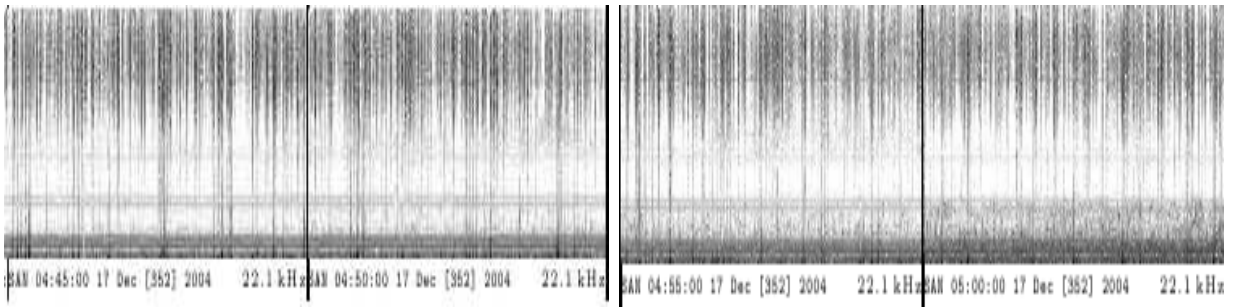


(e) VLF quicklook from 0405-0410UT of 17/12/04 (f) VLF quicklook from 0415-0420UT of 17/12/04

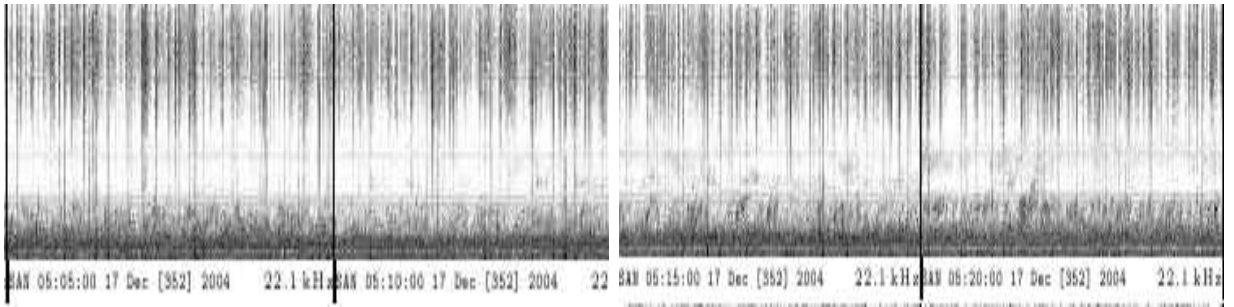


(g) VLF quicklook from 0425-0430UT of 17/12/04 (h) VLF quicklook from 0435-0440UT of 17/12/04

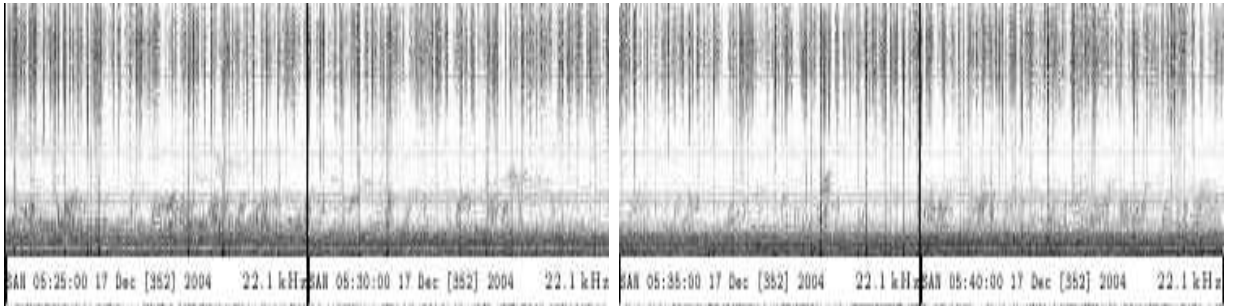
Figure 4.2.2: VLF quicklooks from 0330-0440UT on 17/12/04



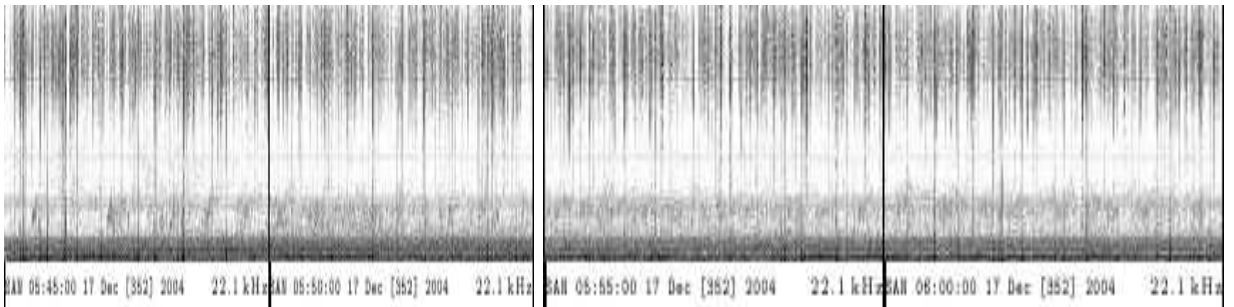
(a) VLF quicklook from 0445-0450UT of 17/12/04 (b) VLF quicklook from 0455-0500UT of 17/12/04



(c) VLF quicklook at 0505-0510UT of 17/12/04 (d) VLF quicklook from 0515-0520UT of 17/12/04



(e) VLF quicklook from 0525-0530UT of 17/12/04 (f) VLF quicklook from 0535-0540UT of 17/12/04



(g) VLF quicklook from 0545-0550UT of 17/12/04 (h) VLF quicklook from 0555-0600UT of 17/12/04

Figure 4.2.3: VLF quicklooks from 0445-0600UT on 17/12/04

Figure 4.2.4 shows absorption recorded at Abisko on day 352 of 2004 from 0000 UT to 0700 UT. We are interested in absorption from 0000 UT to 0600 UT which limits our investigation to darkness at the Finnish chain in month number XII (December), see to Figure 4.2.1. Since the MLT at Abisko is 3h 52min later than SANAE, chorus recorded from 0348 UT to 0600 UT in Figures 4.2.2 and 4.2.3 at SANAE will correspond to absorption observed at Abisko from about 2356 UT (previous day) to 0208 UT marked A and absorption at B corresponds to the same UT when chorus is recorded at SANAE. It should be noted that there is absorption for the whole period of observation i.e; from 0000 UT to 0600 UT, but it's amplitude varies. During this time period $Kp = 4^+$.

During the period of chorus observation, there is a 0.24 dB increase in absorption A and a 2.2 dB at B.

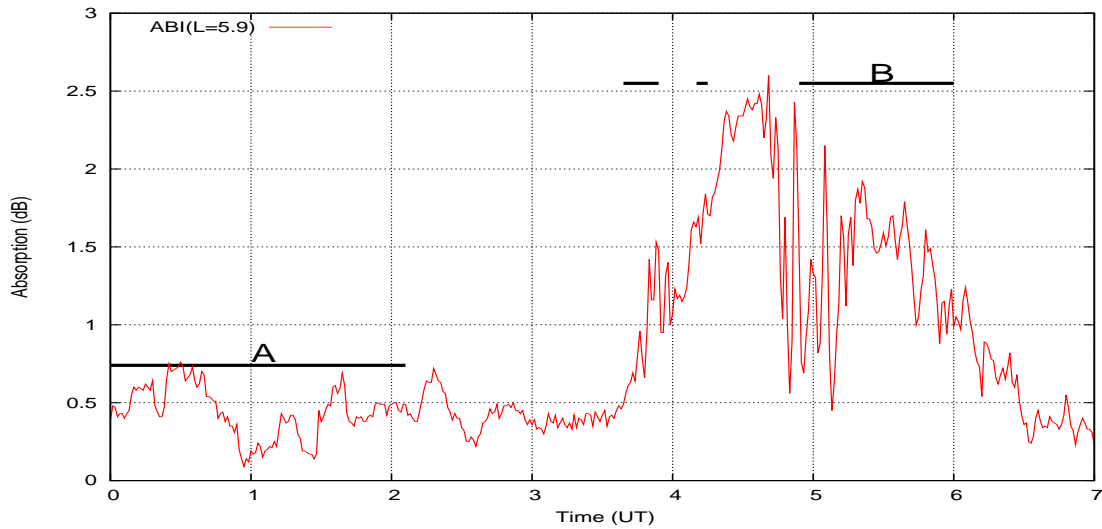


Figure 4.2.4: Riometer Absorption @ Abisko 17/12/04

If the absorption seen at A and B in Figure 4.2.4 is due to chorus, we would want to know how it is related to it's signal intensity. Since the upper boundary frequency of chorus observed here varies between 1 kHz and 2 kHz, we have computed the power spectral density between 1-1.5 kHz and 1.5-2 kHz.

Figure 4.2.5 shows the power spectral density of the VLF signal from 0000 UT to 0700 UT on day 352 of 2004. The intensity is low and steady from 0000 UT to 0330 UT, it varies between 10 and 15 dB/kHz at 1.5-2 kHz whereas at 1-1.5 kHz it varies between 15 and 20 dB/kHz. There is an increase in the VLF signal intensity with the onset of chorus at 0348 UT of 15 dB/kHz in both frequency bands. A 25 dB/kHz increase in the intensity is observed between 0500 UT and 0600 UT. It is evident that the peak in absorption at B in Figure 4.2.4 corresponds to a decrease in the chorus intensity between 0400 UT and 0500 UT shown in Figure 4.2.5. This observation makes it difficult to conclude that chorus recorded at SANAE is related to the observed absorption at B.

A causal effect, however, can not be ruled out as it is probable that the variation of chorus at SANAE, because of the difference in magnetic longitude, does not represent the variation on the Abisko field line.

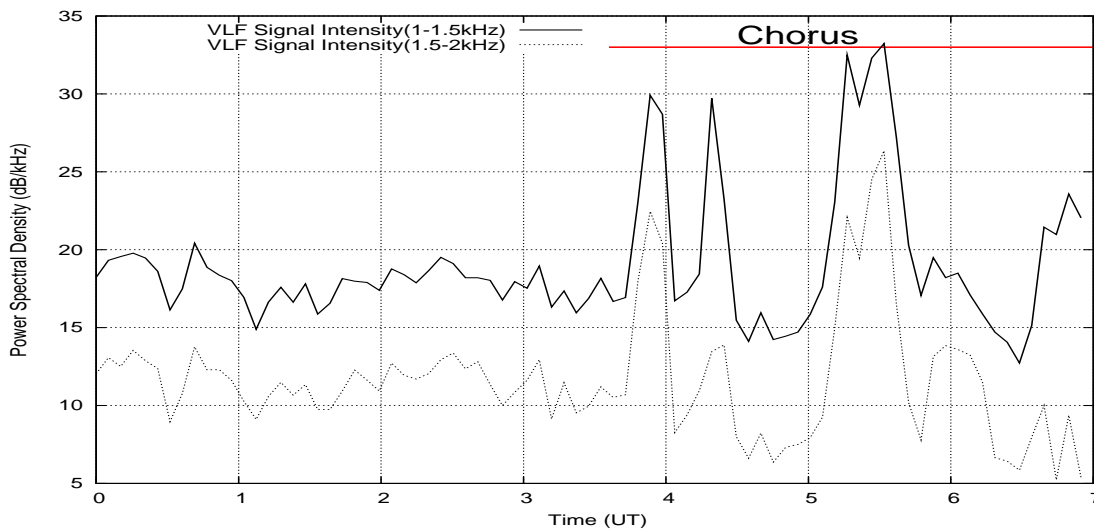


Figure 4.2.5: VLF signal intensity from 0000-0700UT on 17/12/04

The peak in absorption in Figure 4.2.4 corresponds to the time when chorus was off, but it does occur at the same MLT at which chorus is frequently observed at SANAE (refer to the diurnal variation of chorus in chapter 5, Figures 5.2.6, 5.2.7 and 5.2.8.)

Figure 4.2.6 shows absorption recorded at Ivalo from 0000-0700 UT on day 352 of 2004. Like at Abisko, we limit our investigation from 0000 UT to 0600 UT, however since Ivalo' MLT is 4h 19 minutes later than an event observed at SANAE, chorus recorded in Figures 4.2.2 and 4.2.3 shall correspond to absorption from 2329 UT to 0141 UT marked A in Figure 4.2.6, whereas absorption at B corresponds to the same UT when chorus is recorded from 0348-0600 UT at SANAE.

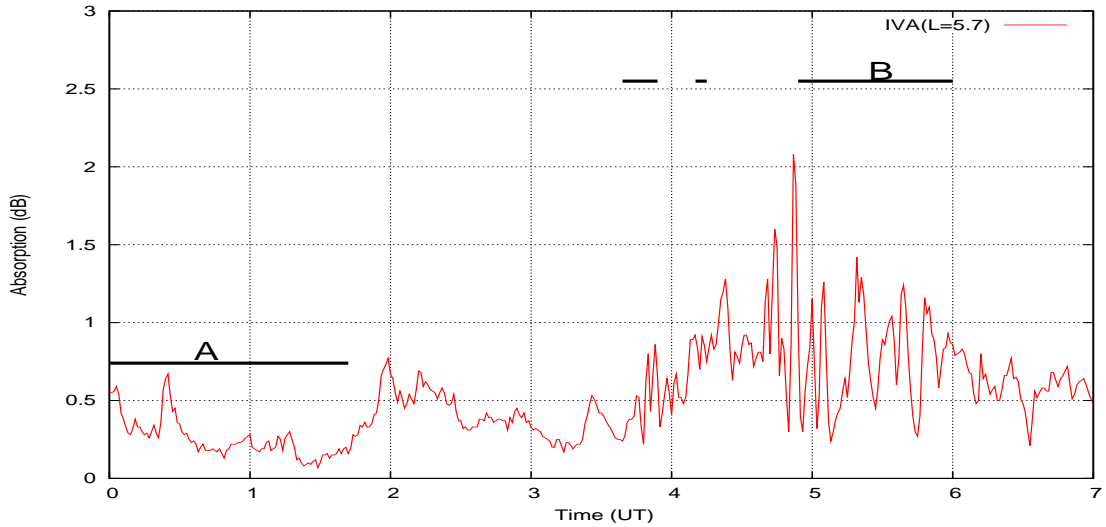


Figure 4.2.6: Riometer Absorption @ Ivalo 17/12/04

Comparing the nature of absorption for the two cases in Figure 4.2.6, we note that there is a decrease in absorption at A($Kp = 4^+$) of 0.50 dB, whereas there is an increase in absorption at B($Kp = 4^+$) of ~ 1.60 dB corresponding to onset of chorus at 0348 UT. Like at Abisko, it is possible that absorption at Ivalo is related to chorus.

If our assumption that observed absorption in Finland at the same MLT (3h to 4h later) as chorus recorded at SANAE is due to chorus enhanced absorption (first method) is true, it would imply that we expect to see a higher absorption at Abisko as compared to that recorded at Ivalo because Abisko is earlier in MLT and as such electron precipitation is expected to be seen earlier than at Ivalo. We have observed that there is a small amount of absorption at the time marked A at Abisko and a decrease at Ivalo for the same chorus event observed at SANAE which is in agreement with the assumption but is not conclusive.

Figure 4.2.7 shows absorption recorded at Sodankylä from 0000 UT to 0700 UT on the same day as earlier cases. Since the MLT at Sodankylä is 4h 12min later than SANAE, the chorus recorded at SANAE from 0348 UT to 0600 UT will correspond to absorption in Figure 4.2.7 from 2336 UT to 0148 UT marked A. With this in mind we look at the nature of absorption at A and compare it to that at B. There is a huge decrease in absorption at A for Sodankylä unlike at Abisko and Ivalo. Refer to Figure 4.2.5 which shows how the signal intensity here affects absorption as compared to that observed earlier. It is clear that intensity of the chorus signal influences enhanced absorption as before.

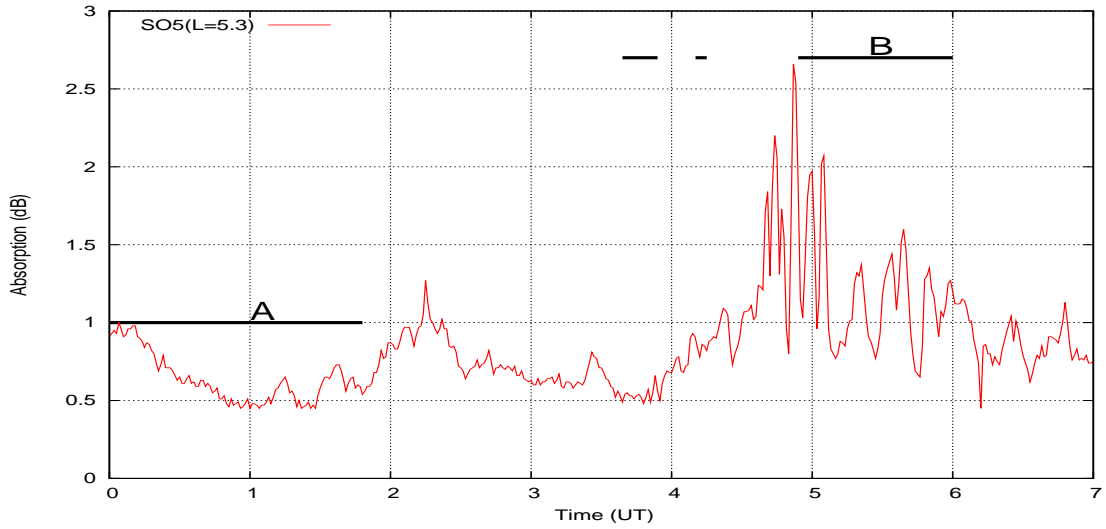


Figure 4.2.7: Riometer Absorption @ Sodankylä 17/12/04

An event observed at Rovaniemi is later than when it is observed at SANAE by 4h 09min in MLT, thus chorus recorded on day 352 of 2004 from 0348 UT to 0600 UT will correspond to absorption recorded at Rovaniemi from 2339 UT to 0151 UT marked A, where absorption marked B corresponds to the same UT as the chorus observed at SANAE, as shown in Figure 4.2.8.

Figure 4.2.8 shows absorption recorded at Rovaniemi from 0000 UT to 0700 UT and it is clear that there is still a remarkable amount of absorption seen between 0348-0600 UT similar to that recorded at other stations. This absorption corresponds to the same universal time when chorus is observed at SANAE, here it is ~ 1.3 dB at B, whereas there is a decrease in absorption at A of 0.38 dB.

Chorus enhanced absorption increases even when chorus switches off at the same universal time when chorus is recorded at SANAE and this possibility relates to a MLT when chorus is frequently observed at SANAE, refer to the diurnal variation of chorus at SANAE in chapter 5.

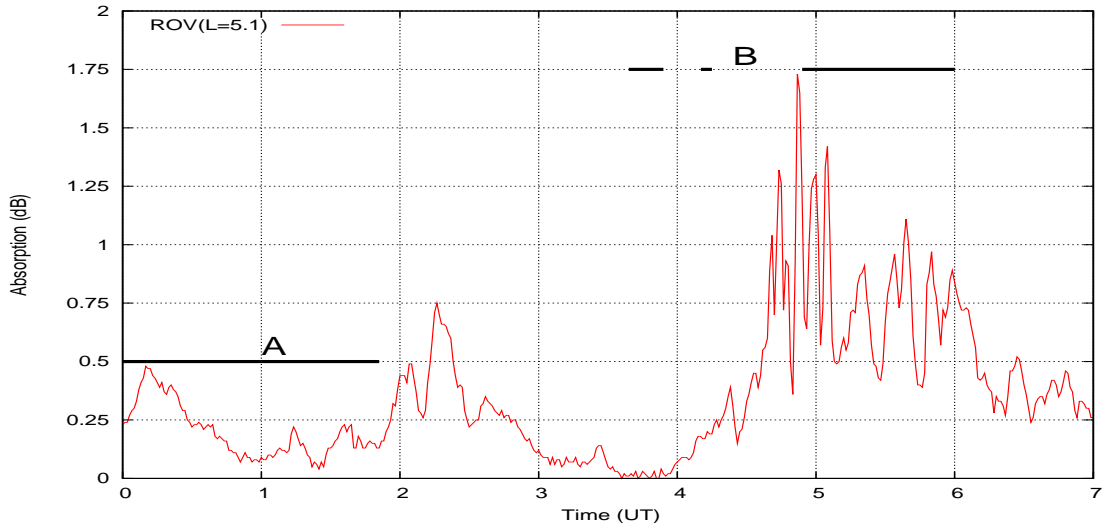


Figure 4.2.8: Riometer Absorption @ Rovaniemi 17/12/04

Oulu is 4h 05min later in MLT than an event observed at SANAE, therefore chorus recorded at SANAE from 0348 UT to 0600 UT on day 352 of 2004 will correspond to absorption from 2343 UT to 0155 UT marked A shown in Figure 4.2.9 and absorption at the same UT when chorus recorded at SANAE is marked B. Unlike absorption results shown earlier, there is absolutely no absorption recorded at A (not even a decrease), whereas there is a 0.14 dB increase at B.

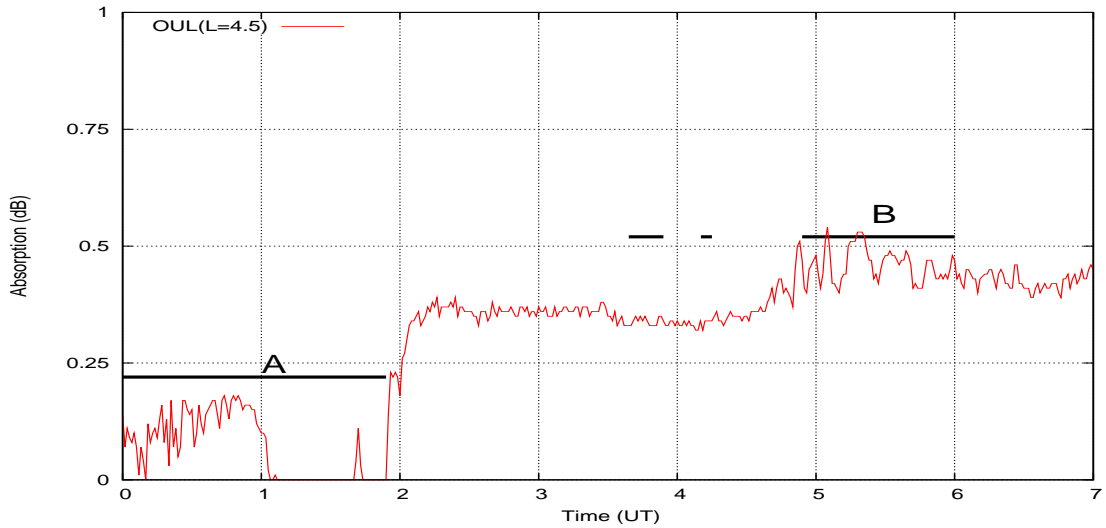


Figure 4.2.9: Riometer Absorption @ Oulu 17/12/04

Comparing absorption at A and at B for all stations used, we note that there is

always more absorption at B than at A and its amplitude generally increases with increasing L-value (see Figure 4.2.10).

Figure 4.2.10 shows the variation of absorption at B with L-value, which increases from 0.4 dB at Oulu with L=4.5 to 1.7 dB at Sodankylä. It drops by 0.10 dB at Ivalo and peaks to 2.2 dB at Abisko with L=5.9. The increase in absorption with increasing L-value suggests that, if this absorption is indeed due to chorus induced electron precipitation, then the region of maximum chorus generation may lie on higher L-shells than SANAE.

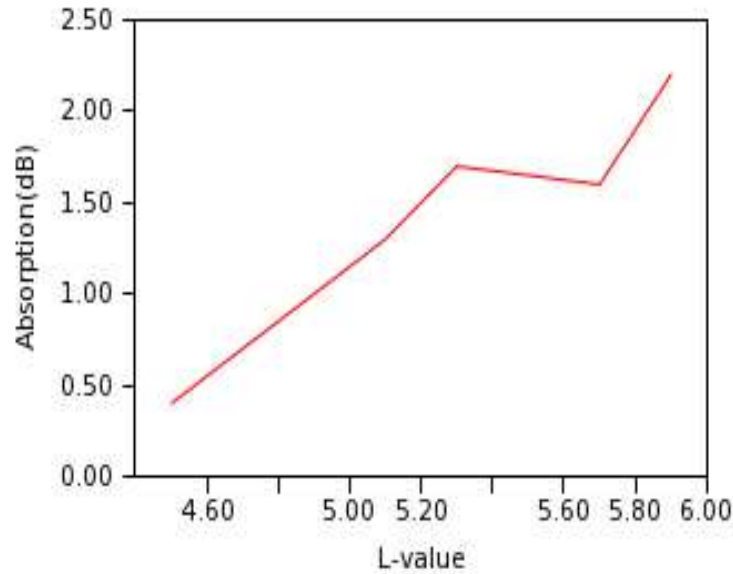


Figure 4.2.10: Absorption vs L-value @ 'B' for 24/01/04

The results presented above do not offer any proof that there is an association between chorus and absorption in the opposite hemisphere.

Spectrograms in Figure 4.2.11 show quicklooks recorded on day 275 of 2005 from ~0030-0505 UT. The signature has a constant upper boundary frequency, it switches on and off during this period.

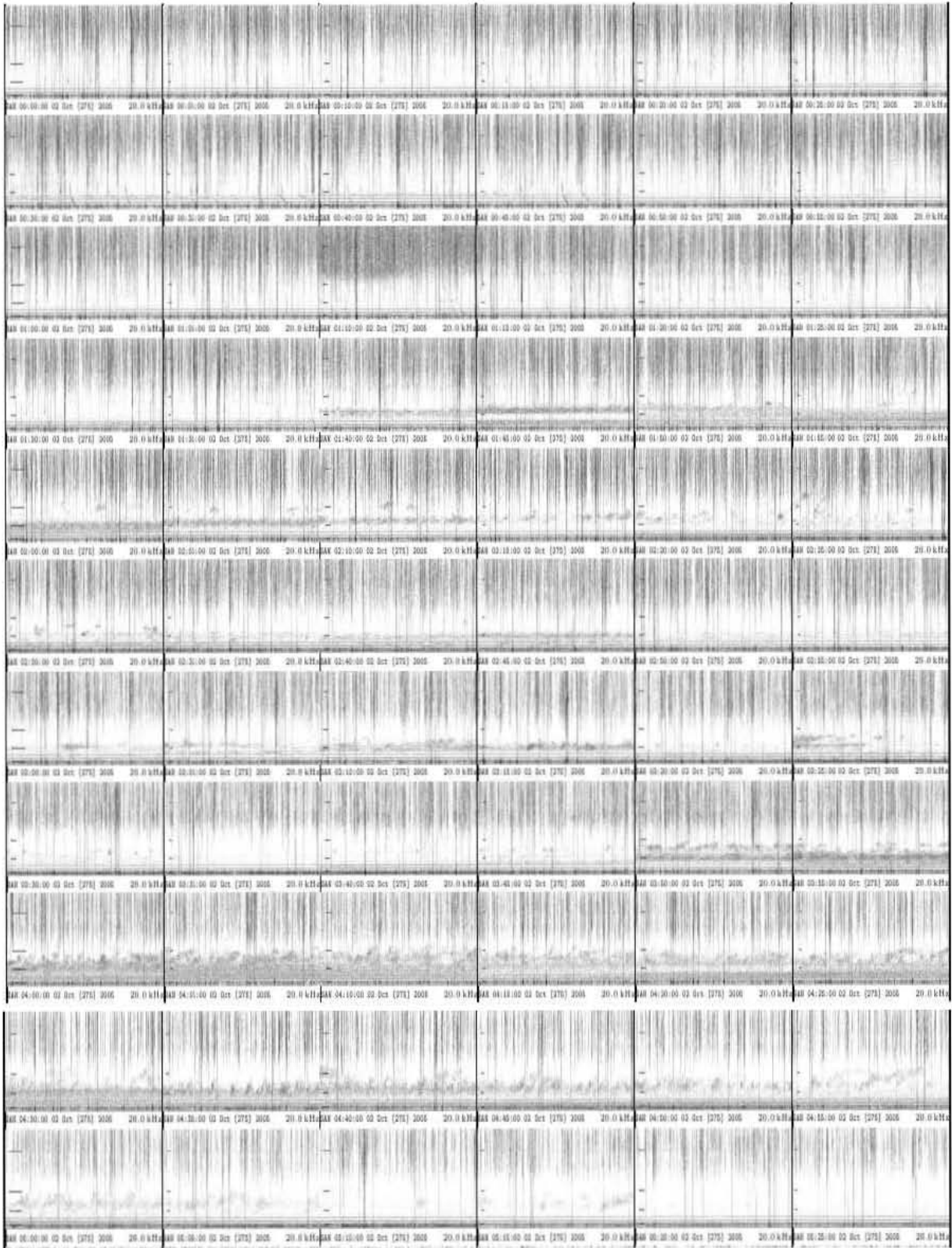


Figure 4.2.11: VLF quicklooks from 0000-0500UT on day 275 of 2005

Figure 4.2.12 shows absorption at Ivalo from 0000 UT to 0700 UT on day 275 of 2005. The horizontal lines marked B indicate simultaneous observations with chorus at SANA E. The spaces in between the marks show chorus switching off. In order to limit our observation to darkness only, we restrict our time of observation from 0000 UT to 0400 UT. We reached this result because the Local Time (LT) in Finland is 2 hours later than the Universal Time (UT) and darkness on day 275 extends to 0600 LT \sim 0400 UT.

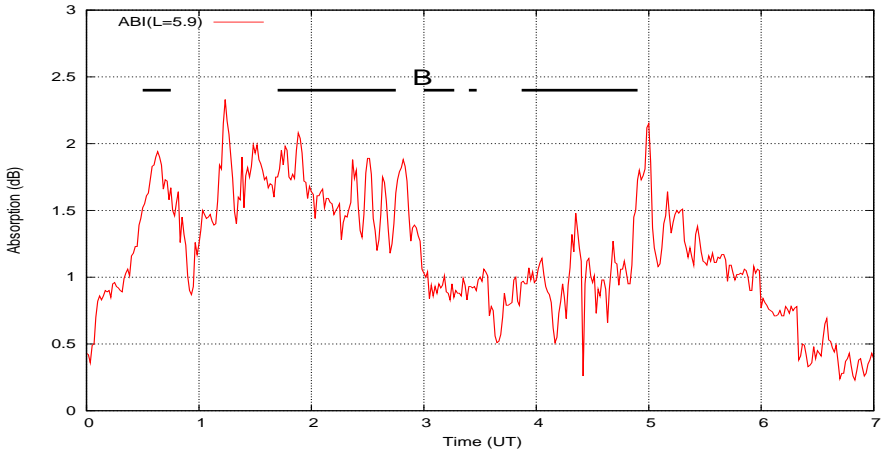


Figure 4.2.12: Absorption @ Abisko on 02/10/05

Chorus enhanced absorption at Abisko generally increases with the switching on of chorus and decreases with the switching off of chorus and varies between 1 and 2.4 dB.

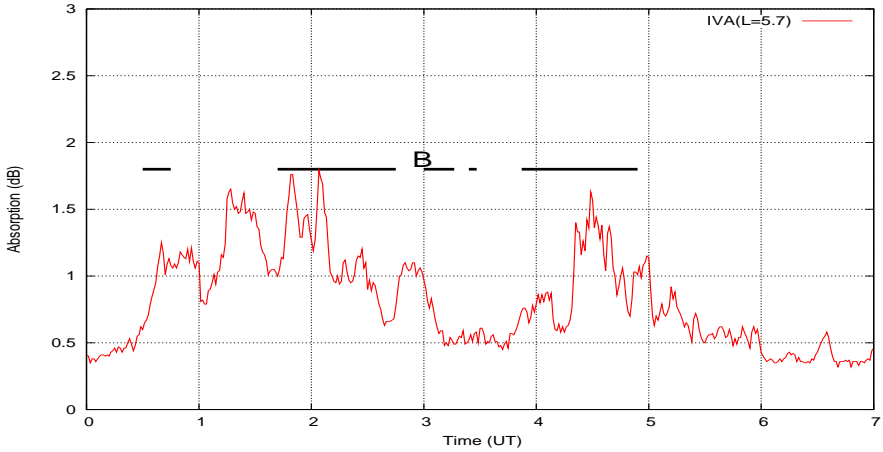


Figure 4.2.13: Absorption @ Ivalo on 02/10/05

In Figure 4.2.13, we show how absorption at Ivalo varies with chorus recorded at

SANAE on the same day as in the previous case. It is clear that enhanced absorption at Ivalo also varies with the switching on and off of chorus and is confined to 0.6-1.8 dB.

Figure 4.2.14 shows absorption at Sodankylä on day 275 of 2005 between 0000 UT and 0700 UT, we limit our investigation to 0000-0400 UT for the reasons given earlier.

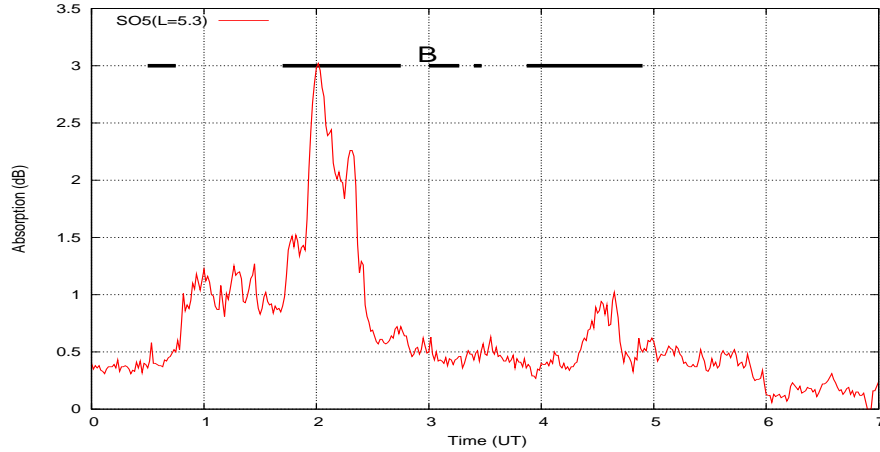


Figure 4.2.14: Absorption @ Sodankylä on 02/10/05

There is a remarkable increase in absorption when chorus is on at precisely 0200 UT for Sodankylä of 3 dB as compared to a much lower absorption observed at the same time for the other stations.

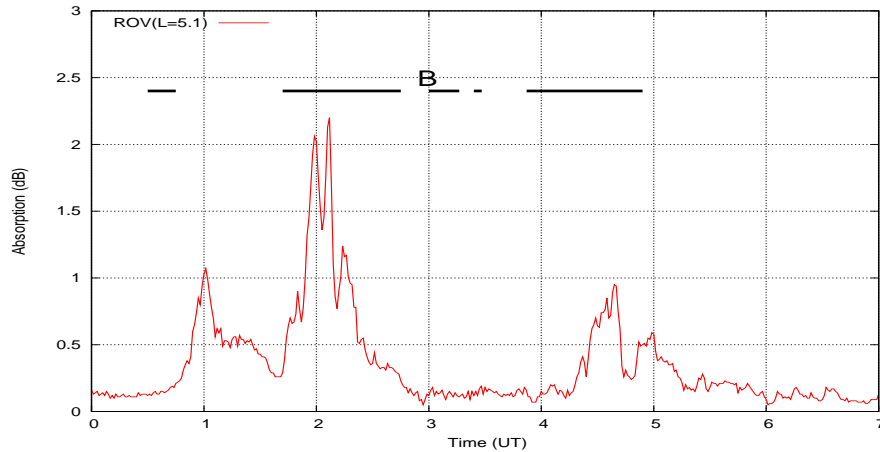


Figure 4.2.15: Absorption @ Rovaniemi on 02/10/05

Absorption at Rovaniemi on day 275 of 2005, as shown in Figure 4.2.15, varies between 0.1 and 2.4 dB. The absorption generally increases and decreases with the

switching on and off of chorus respectively. However, this result is inconclusive because there are times when we have observed peaks in absorption when chorus is off.

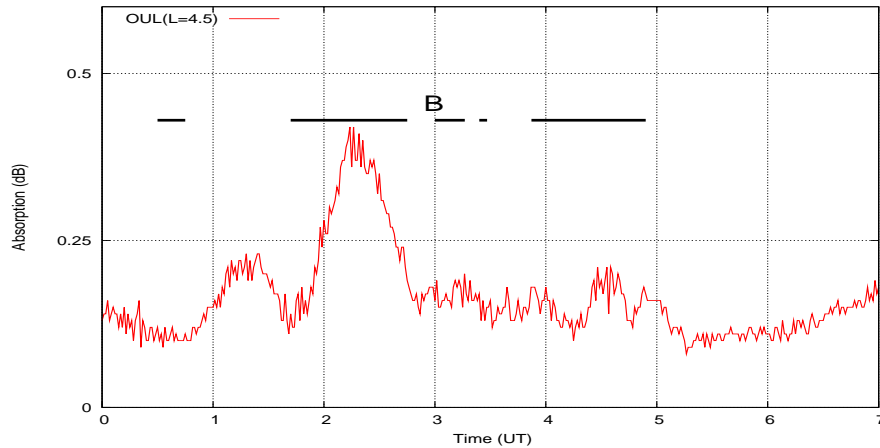


Figure 4.2.16: Absorption @ Oulu on 02/10/05

Chorus enhanced absorption at Oulu on day 275 of 2005 is generally below 0.5 dB but increases and decreases with the switching on and off of chorus respectively.

4.3 Conclusions

For the two case studies we have presented there is no clear association between absorption and chorus. There are however two indications that a connection may exist.

1. Increased absorption occurs at an MLT when the probability of chorus occurring is high. The maximum absorption in case 1, for example, occurs between 0400 and 0500 UT and this at the Finish chain corresponds to about 0600 and 0700 MLT.
2. Absorption varies in longitude in a way that might correspond to the switching on and off of chorus.

With these features in mind we consider in the next chapter the probability of the occurrence of chorus during the day and with season.

Chapter 5

VLF Statistics

5.1 Introduction

Since 2002, continuous broadband VLF recordings have been made remotely at SANAE [71°40'S 2°50'W, $L = 4.3$] using a Digital VLF Recording and Analysis System (DVRAS). The system consists of two perpendicular magnetic loop antennae. The loops are oriented geomagnetic north-south and east-west and each has an area of 100 m². This allows the arrival azimuth of a signal to be found. The VLF signals are amplified and then digitised at a sampling frequency rate of 44.1 kHz using a 16 bit sound-card in a personal computer (PC). The PC time is synchronised with the Pulse Per Second (PPS) signal from a GPS receiver. The PPS timing accuracy is better than 1 μ s, which is much smaller than the data sampling period 22 μ s. The data are recorded for 1 minute in 5 throughout the year. This means that there is a 4 minute data gap from one event to the next.

The digitised data are stored on a PC as wav files and only returned to Durban at the end of each year. Each wave file is a stereo of the signal from channel 1(north-south loop) and channel 2(east-west loop) and we have used data from channel 2 because of it provided a better signal quality and was much more stable. However, VLF quicklooks are sent on a daily basis from the recording system in Antarctica to the Space Physics Research Institute in South Africa via satellite and it was these quicklooks that were used to do the statistics presented here. VLF quicklooks are frequency-time graphs and are used to identify the particular VLF phenomena. The statistics presented in this chapter are for the years 2002, 2004 and 2005. Various VLF emission signatures were identified in the data such as hiss, chorus, falling tones, risers, hooks, triggered

emissions, periodic and quasi-periodic emissions. Whistlers and whistler echo trains were also recorded. Detailed analyses were done for the chorus emission and whistlers.

5.2 VLF Chorus Statistics

Chorus may be observed at any local time at SANAE but it occurs predominantly between 0600 and 1300 local times (LT). The longitude of SANAE is close to zero, the Universal and Local Times are nearly the same, but magnetic midnight local time (MLTMN) is 1 hr 45 minutes earlier than the local time.

Chorus is principally generated in two magnetic latitude regions as shown in Figure 5.2.1. These regions are namely the equator (equatorial chorus), and on high L-shells at about 15° [Tsurutani and Lakhina, 1997]. Figure 5.2.1 is a schematic representation of the magnetic field in the noon-midnight meridian plane based on the magnetosphere field model of Mead and Fairfield, [1975] showing the generation regions.

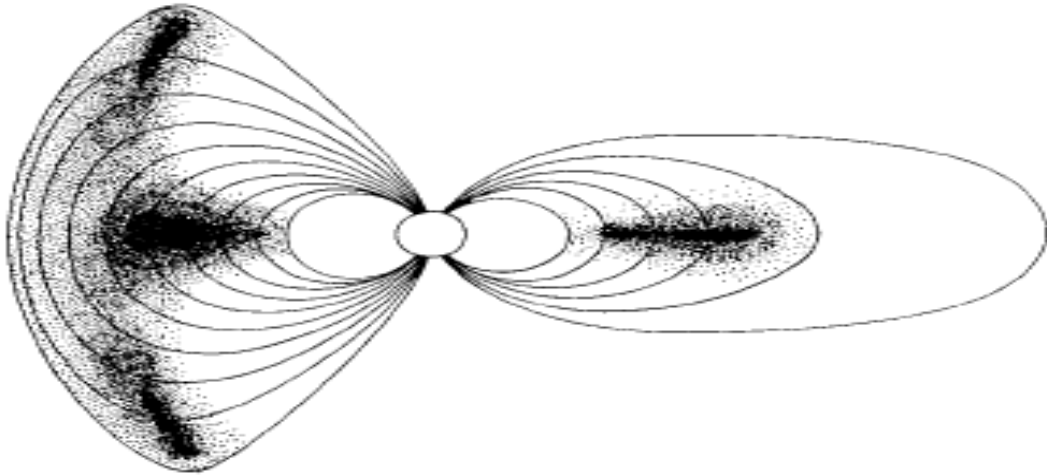


Figure 5.2.1: From *Tsurutani and Smith* [1977, Figure 14].

The density of the dots indicate the regions where chorus is likely to be generated. The higher the density the greater the generation probability. Equatorial chorus occurs primarily during substorms, whereas high-latitude chorus is conspicuous during quiet times [Tsurutani and Lakhina, 1997]. The chorus recorded at SANAE is generated at the equator.

Spectrograms presented in Figures (5.2.2 -5.2.5) are examples of chorus emissions recorded at SANAE. These figures are generated by computing the windowed discrete-

time Fourier transform of a signal using a sliding window or short-time Fourier transform (STFT). This method looks at a small section or window of the signal, finds frequencies within this window and then maps the signal onto a two-dimensional function of frequency-time.

Chorus is a series of rising tones usually ranging from about 2 kHz to 3.9 kHz at SANAE. The lower boundary may be determined by propagation in the earth-ionosphere wave guide where the waves have entered the atmosphere at some distance from the station whereas the upper cut-off frequency is probably determined by the limit of ducted propagation in the magnetosphere. Smirnova [1984] has used the upper cut-off(f_{UB}) to locate the generation region. Smirnova assumes that the chorus is generated in the equatorial plane and its upper frequency therefore determines the L-shell on which it was generated. In a dipole field the equatorial gyrofrequency is given by $f = 880 \text{ kHz}/L^3$.

Thus, f_{UB} will give the L-value of the source as shown in Equation 5.2.1 where f_{UB} is in kHz.

$$L = (440/f_{UB})^{1/3} \quad (5.2.1)$$

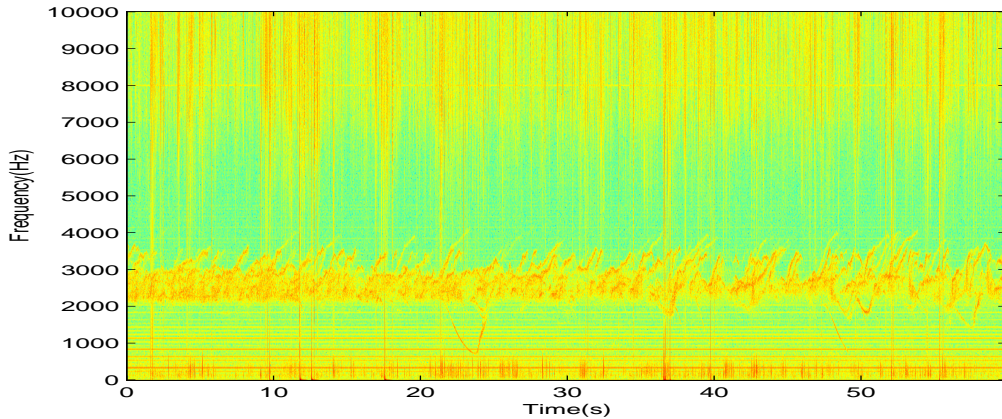


Figure 5.2.2: 15:10 UT 31 January 2004

Figures 5.2.2 to 5.2.5 are spectrograms recorded at SANAE on 31 January, 2004 which show that chorus may vary in a short period of time. In Figure 5.2.2 the signature is seen to lie between 2 kHz and 3.7 kHz with hooks below 2 kHz at ~ 24 sec and several others beyond ~ 36 sec. The hooks seen at two different frequencies may be due to cyclotron resonance on different L-shells.

The vertical lines are sferics and are as a result of the undispersed lightning signal propagating in the Earth-ionosphere wave guide. The chorus in Figure 5.2.2 has $f_{UB} = 3.7$ kHz, giving an L-value for the source region of 4.9.

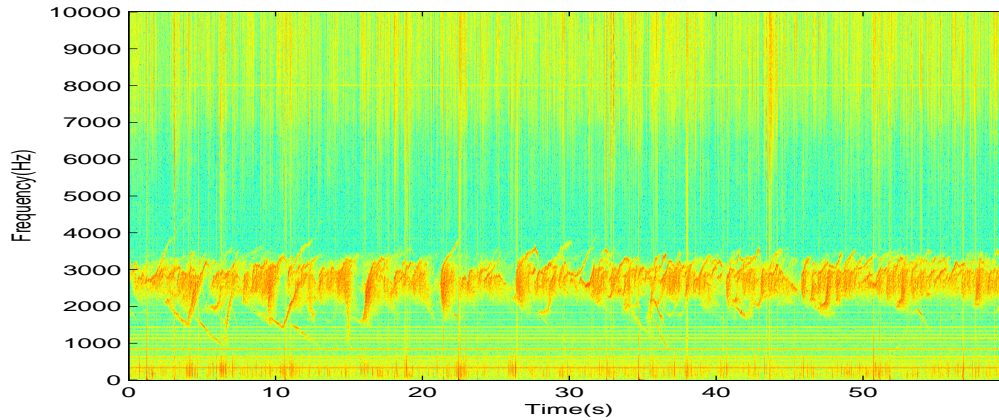


Figure 5.2.3: 15:20 UT 31 January 2004

Figure 5.2.3 shows chorus observed on the same day but 10 minutes later than that shown in Figure 5.2.2, the chorus is seen to be more intense than before and there are larger hooks below 2 kHz in the first 20 sec. However, the f_{UB} is observed to have dropped by 0.2 kHz than that recorded 10 minutes earlier giving a source of $L = 5.0$.

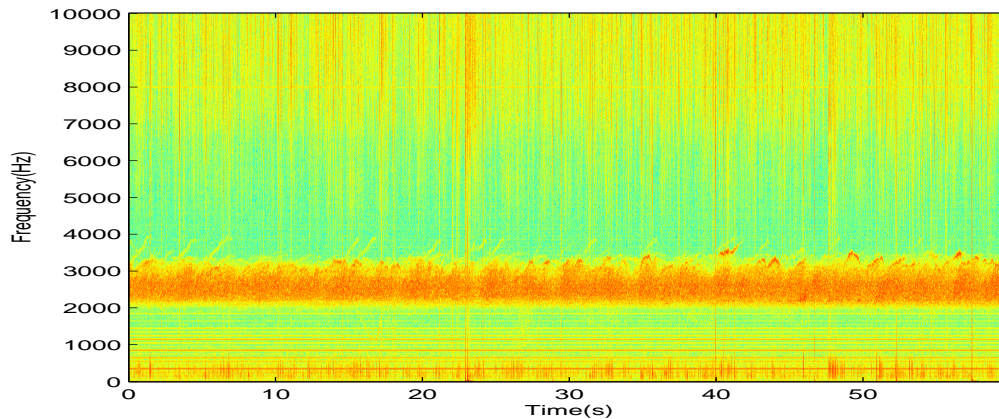


Figure 5.2.4: 15:30 UT 31 January 2004

The chorus event in Figure 5.2.4 is superimposed on the hiss signature with no hooks, here the chorus elements are seen to have an $f_{UB} \sim 3.9$ kHz implying that the L_{source} would be at 4.8.

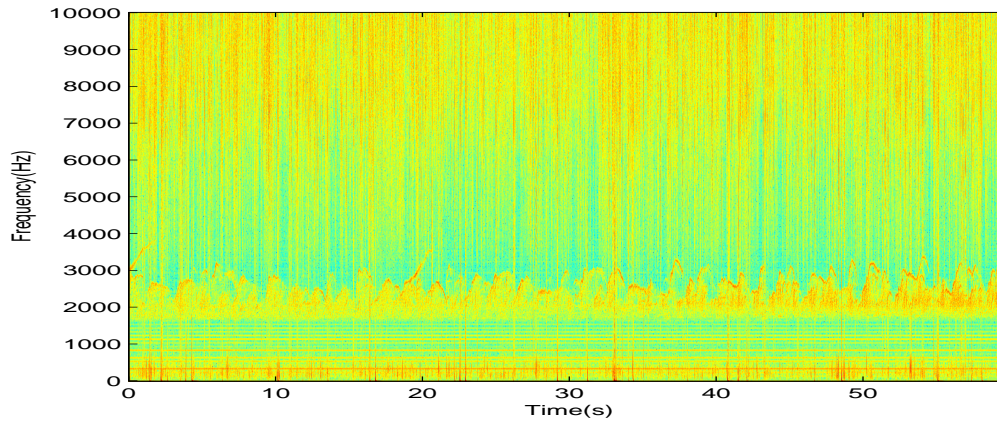


Figure 5.2.5: 17:05 UT 31 January 2004

Figure 5.2.5 shows a chorus signature recorded on day 031 of 2004 with ~ 1.8 kHz lower bound frequency and having an f_{UB} of ~ 3.2 kHz without any hooks. Using Equation 5.2.2 as before, the L_{source} for this event is found to be 5.2.

The factor that controls the observed chorus frequencies is the equatorial gyrofrequencies [Burtis and Helliwell, 1969].

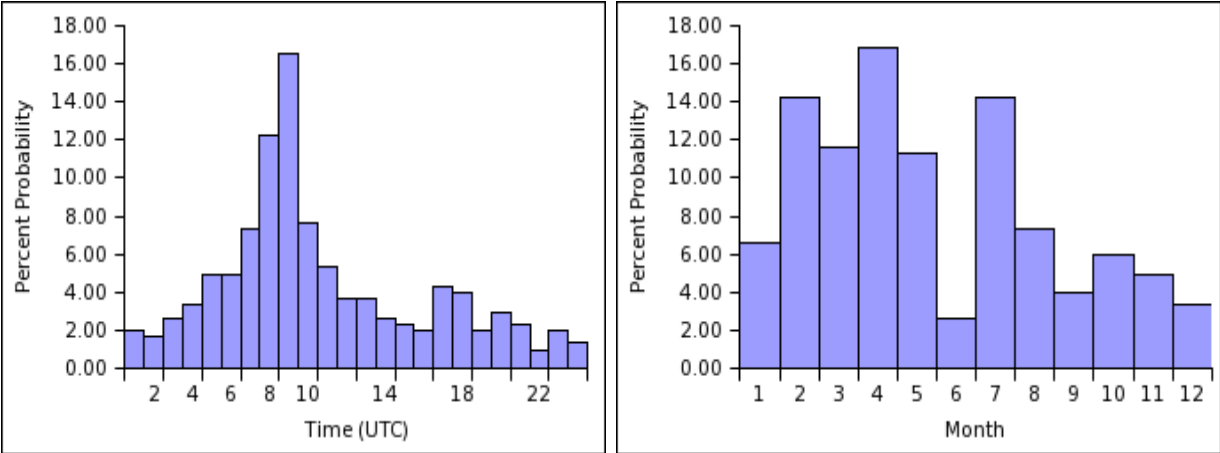
It appears using these methods, that the chorus recorded at SANAE is generated on higher L-shells than the station.

We have derived statistics for the diurnal and seasonal occurrence of chorus for the years 2002, 2004 and 2005 using quicklooks. In these statistics, if chorus is recorded at any time in a particular hour it is counted as a 1 and if it is not, it is counted as 0. This was done for every hour of the day throughout the whole year to give the diurnal variation. We have data for 21914 hours and chorus was recorded in ~ 1950 hours of these, with 952 hours as the highest recorded in 2004 followed by 688 hours in 2005 and 310 hours in 2002 as the lowest. A diurnal average was then obtained over a year for all three years' data taking into account the number of days on which the receiver was not operational in that particular year.

The mean diurnal percent probability of observing chorus was obtained by averaging the frequency of recording chorus in a given hour over a year using Equation 5.2.2 below.

$$P = \frac{N_c}{N_T} \times 100\% \tag{5.2.2}$$

where P is the percent probability, N_c is the frequency of a particular hour recording chorus in a year and N_T is the total number of observing hours in a year.



(a) Diurnal variation of VLF chorus

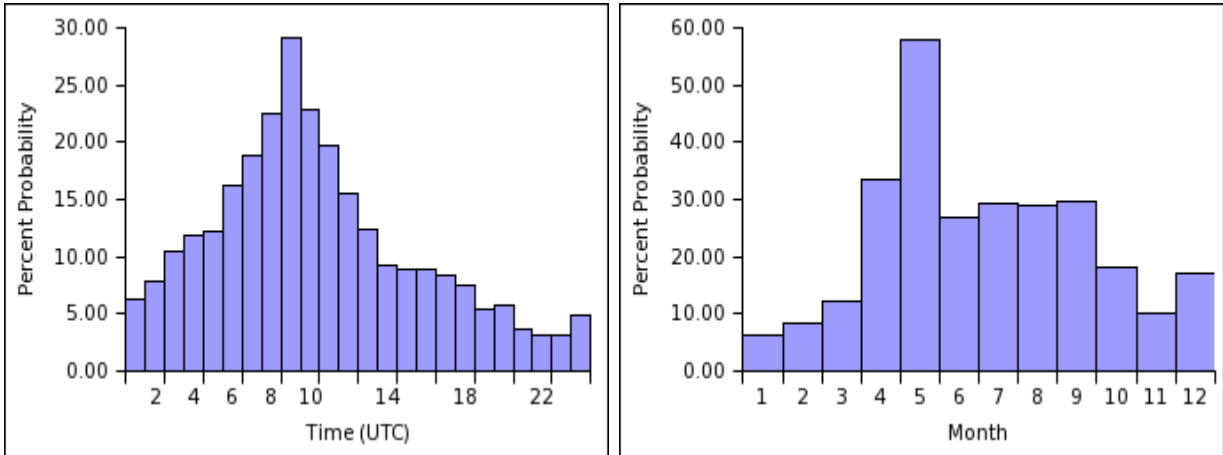
(b) Seasonal variation of VLF chorus

Figure 5.2.6: Diurnal and Seasonal variation of chorus for the year 2002 at SANA E

Figure 5.2.6 shows data obtained from quicklooks at SANA E for the year 2002 using binary statistics, with the diurnal variation of the signature in (a) showing a high probability of observing chorus between 0600 UT to 1000 UT and a maximum probability between 0800 and 0900 UT corresponding to an MLT of about 0600 to 0700 . The diurnal percent probability begins to rise right from midnight reaching a peak of between 16% and 18% between 0800 UT and 0900 UT. It then begins to drop from

this max until midnight when it starts to increase again. Figure 5.2.6(b) presents the seasonal variation for chorus in the same year, which varies continuously throughout the year with a max percent probability between 16% and 18% in April.

Figures 5.2.7 (a) and (b) show the diurnal and seasonal variation of observing chorus at SANAE for the year 2004 respectively. The diurnal variation has $> 10\%$ probability of observing chorus between 0300 UT and 1300 UT, and has a peak of $\sim 30\%$, much higher than that seen in 2002 but interestingly observed at the same UT. Like in Figure 5.2.6(a), the diurnal percent probability of observing the signature starts to rise from midnight UT peaking between 0800 UT and 0900 UT and begins to drop until midnight.



(a) Diurnal variation of VLF chorus

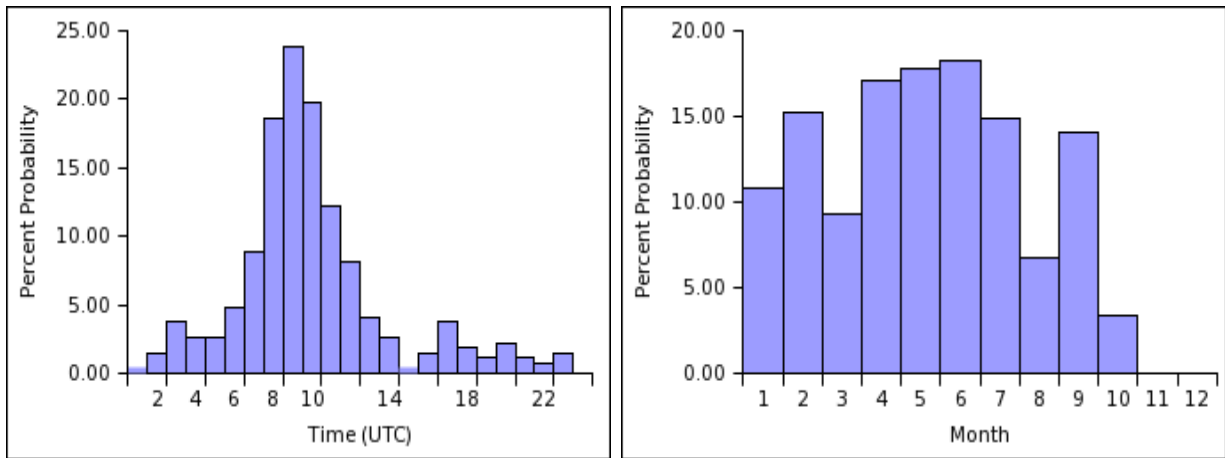
(b) Seasonal variation of VLF chorus

Figure 5.2.7: Diurnal and Seasonal variation of chorus for the year 2004 at SANAE

Figure 5.2.7(b) shows the seasonal variation of chorus observed in 2004 at SANAE, which varies continuously throughout the year with a max percent probability of observing the signature of $\sim 60\%$ in May.

Figure 5.2.8 shows in (a) the diurnal and (b) seasonal variation of observing chorus for the year 2005. The diurnal max percent probability of observing chorus was found to be $\sim 25\%$ between 0800UT and 0900 UT, however, it has a $> 10\%$ probability between 0700 UT and 1000 UT. As observed in 2002 and 2004, the percent probability starts to rise from midnight peaking exactly between 0800 UT and 0900 UT and begins to drop until midnight.

Figure 5.2.8(b) presents the seasonal variation of observing chorus at SANAE with a max percent probability of $\sim 20\%$ in June with nothing observed in November and December for no availability of data. The seasonal percent probability of observing chorus here is similar to that observed in 2002 and 2004.



(a) Diurnal variation of VLF chorus

(b) Seasonal variation of VLF chorus

Figure 5.2.8: Diurnal and Seasonal variation of chorus for the year 2005 at SANAE

Even though we have only worked on 3 years' data, it is evident from all the years here that chorus' diurnal variation interestingly seems to follow a pattern. The diurnal percent probability starts to rise right from midnight peaking between 0800 UT and 0900 UT and immediately begins to fall until midnight again when it begins to rise.

All the three years data worked on have a maximum between 0800 UT to 0900 UT as can be seen from Figures 5.2.6, 5.2.7 and 5.2.8. It can be noted from these graphs therefore that the VLF chorus emission is a morning signature confirming the name *Dawn Chorus*.

The seasonal variation has a high probability of observing chorus in the winter months when the ionosphere is most transparent to the reception of VLF waves.

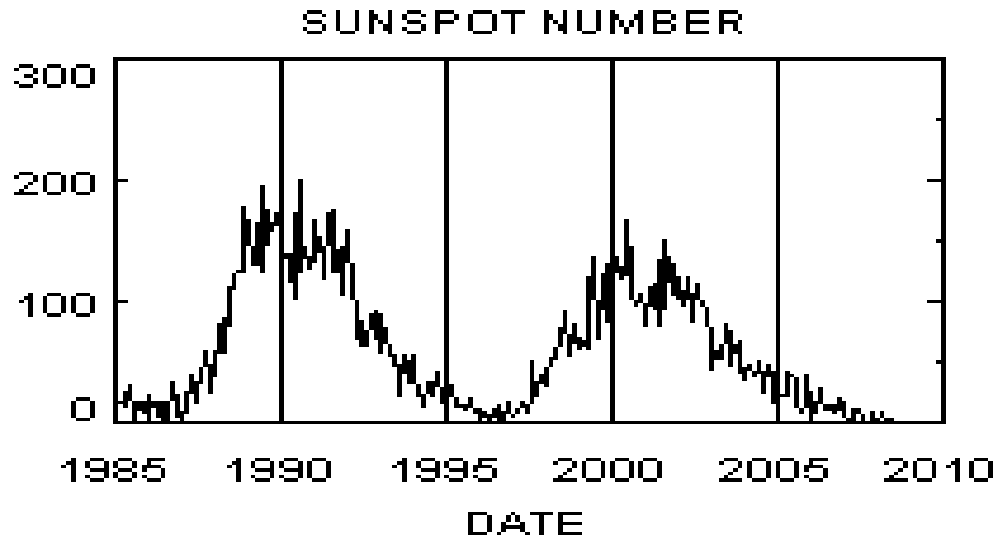


Figure 5.2.9: Sunspot cycle [http://science.nasa.gov/headlines/y2006/21dec_cycle24.htm]

Figure 5.2.9 reflects the Solar cycle from the year 1985 to the year 2008 computed using monthly averages. We are generally interested in the years beyond 2000 which coincide with the years for the data used in this thesis. It can be seen that the sunspot number decreases from the year 2000 up to date which implies that there is a reduction in the number of energetic particles entering the geospace environment. We do know however that the falling side of the solar cycle corresponds to an increase in the geomagnetic activity.

To see if in fact chorus occurrence is influenced by geomagnetic activity we have examined the Dst index which gives a measure of the equatorial ring current particle fluxes.

Figure 5.2.10 shows the variation of the Disturbance Storm Time ‘Dst’ index from 2002 to 2005, the index measures the level of induced ring currents, perturbations in the magnetic fields and enhanced particle fluxes in space which is what we are interested in. The figure shows that there was a greater magnetic activity in 2004, less in 2005 and least in 2002.

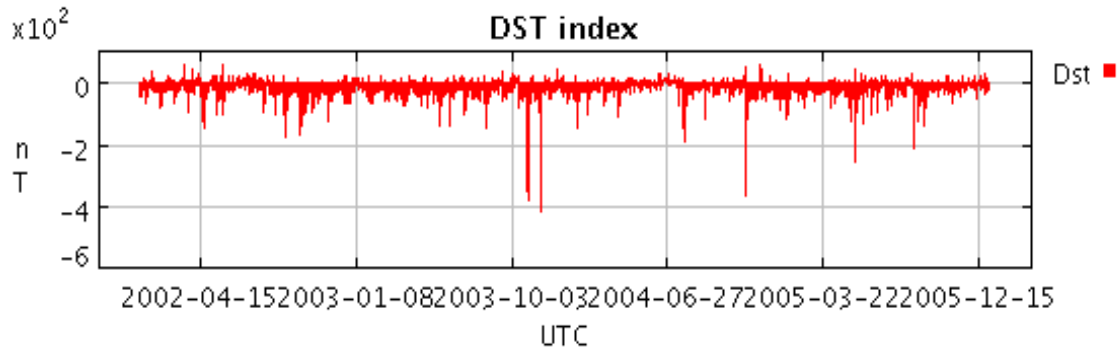


Figure 5.2.10: Dst index from 2002-2005[<http://spidr.ngdc.noaa.gov/spidr>]

The seasonal variation of the chorus as can be seen in Figures 5.2.6b, 5.2.7b and 5.2.8b varies throughout the year with $\sim 18\%$ in April, 2002 when the magnetic activity is lowest (Sunspot number is highest), $\sim 60\%$ in May, 2004 when the magnetic activity is highest and $\sim 20\%$ in June, 2005 when the magnetic activity is low (with lowest Sunspot number) in the 3 years of chorus observations. It is interesting to observe an increase in percent probability of observing chorus with an increase in the Dst index as shown in Figure 5.2.10. It can be concluded therefore that the diurnal and seasonal variation of chorus at SANAE does not seem to be influenced by the solar cycle but definitely is influenced by the Dst index.

From the 3 years’ chorus data, the highest percent probability of seasonally observing chorus at SANAE is in winter months. This is because in winter, SANAE is in the dark making the ionosphere more transparent to the reception of chorus waves.

5.3 Whistler Statistics

A Whistler as described in section 3.4.1 is a descending VLF tone, produced by waves from terrestrial lightning after propagation through the magnetosphere [Storey, 1953]. Lightning is a source of electromagnetic radiation, generating a broad-band pulse which propagates in the VLF range through the atmosphere in the Earth-ionosphere waveguide

The annual and diurnal variation of whistler occurrence were determined by using quicklook spectrograms. We recorded a 1 or 0 for the occurrence or non occurrence of whistlers in a given hour throughout the year. We have data for 21914 hours and whistlers were recorded in ~ 409 hours of these at SANA E for the years 2002, 2004 and 2005 VLF data used. These binary statistics do not account for the actual number of whistlers recorded but simply the likelihood of a particular hour having a whistler. The seasonal and diurnal variation of whistlers have been established for the three years' VLF data. The diurnal variation of whistlers was obtained using the method used for VLF chorus explained in section 5.2.

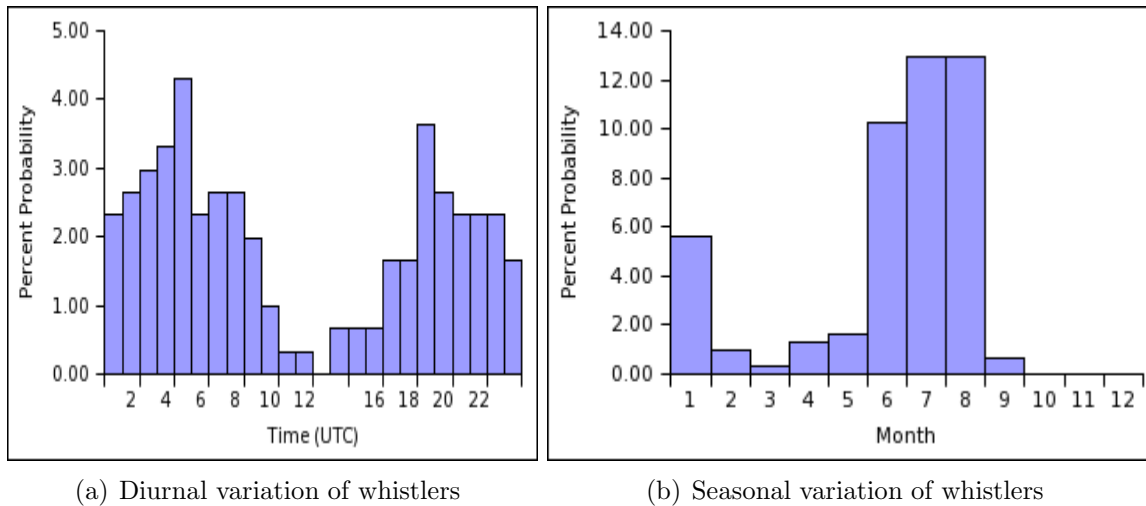
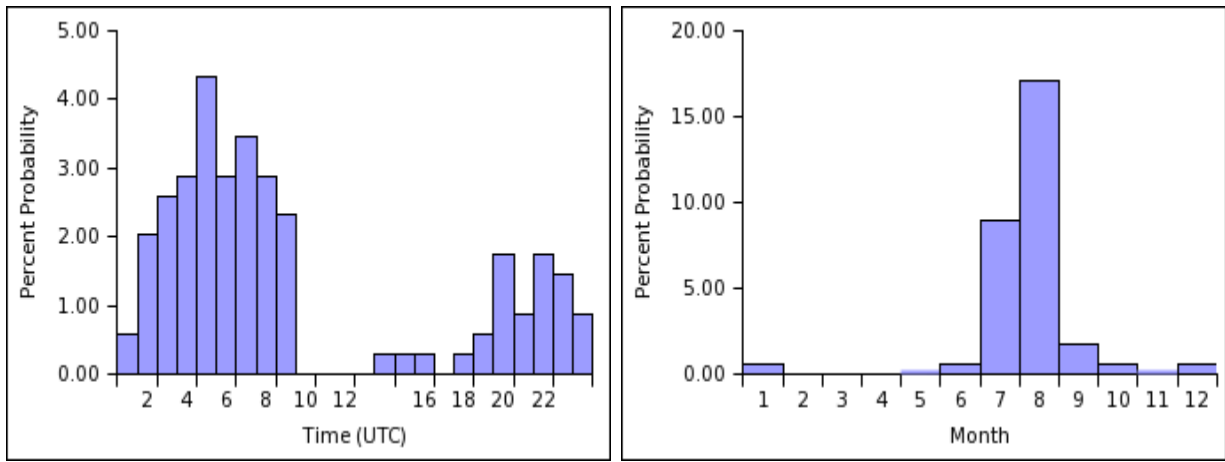


Figure 5.3.1: Diurnal and Seasonal Variation of whistlers for the year 2002 at SANA E

Figure 5.3.1 shows whistler diurnal and seasonal variation statistics for the year 2002 in (a) and (b) respectively. The diurnal variation begins to rise from midnight peaking between 0400 UT and 0500 UT and declines during daylight hours. The probability begins to increase again in the late afternoon.

The seasonal variation shows a high probability of observing whistlers in the winter months, June to August, and a very small probability at any other time of the year.

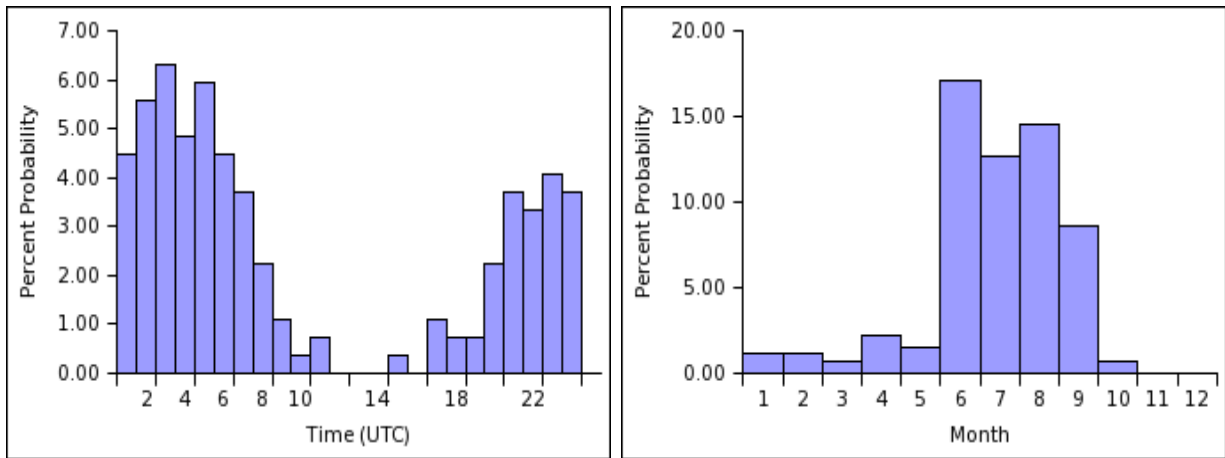


(a) Diurnal variation of whistlers

(b) Seasonal variation of whistlers

Figure 5.3.2: Diurnal and Seasonal Variation of whistlers for the year 2004 at SANAE

Figure 5.3.2 shows the diurnal variation in (a) and the seasonal variation in (b) of observing whistlers at SANAE for the year 2004. As in Figure 5.3.1(a), the diurnal percent probability begins to increase from midnight having its peak between 0400 UT and 0500 UT and drops to almost nothing between 1000 UT and just before evening when it peaks at $\sim 2\%$. The seasonal percent probability is also high between July and August with negligible for the rest of the months.



(a) Diurnal variation of whistlers

(b) Seasonal variation of whistlers

Figure 5.3.3: Diurnal and Seasonal Variation of whistlers for the year 2005 at SANAE

Figure 5.3.3 presents whistler statistics for the year 2005, (a) shows the diurnal percent probability of observing the signature which is similar to that observed in 2002

and 2004. The percent probability is high in the morning sector, declines to nearly negligible between 0900 UT and 1600 UT when it begins to rise again till midnight.

The seasonal variation is significantly high from June to September which is the same period when it is highly observed in the years 2002 and 2004. It should be noted that the seasonal variation percent probability of observing whistlers is well defined between June and September for all the three years statistics.

HOURS OF WHISTLER OBSERVATION			
Year	2002	2004	2005
Max	39	59	46
Min	1	1	2
Avg	11.75	8.83	13.5

Table 5.3.1: Monthly average, max, min hours of whistler observations at SANA E

Whistler observations for the three years VLF data at SANA E have been compiled and it has been observed that 2005 recorded the highest number of ~ 162 hours with a peak in June of 46 hours of observations followed by 2002 with 141 hours with a max of 39 in July and the least being 106 hours recorded in 2004 having a peak in August of 59 hours as shown in Table 5.3.1.

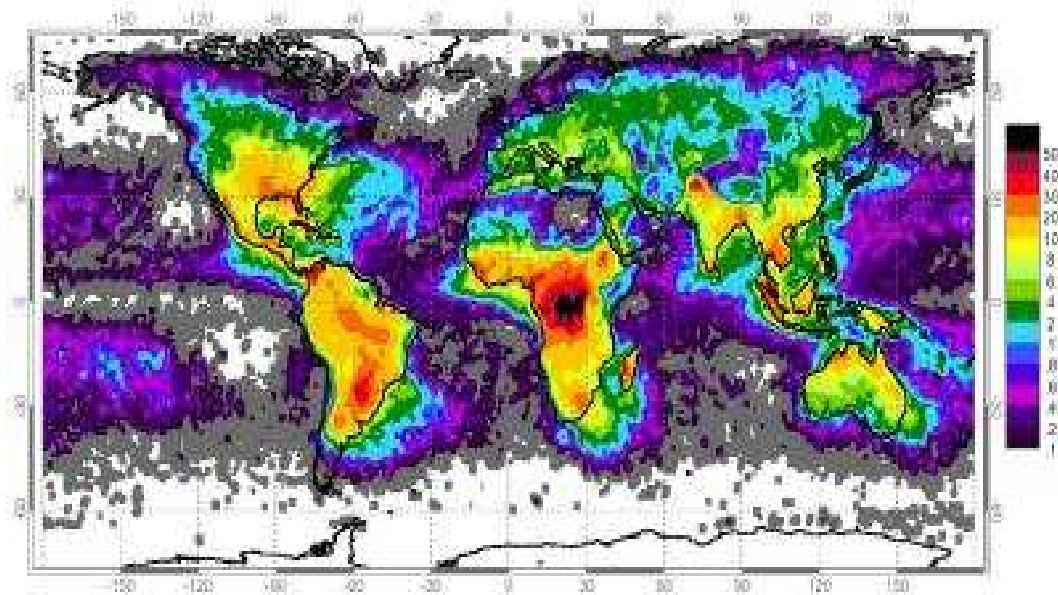


Figure 5.3.4: Lightning Locations <http://cellar.org/showthread.php?t=800>

Figure 5.3.4 shows the least and most lightning locations world wide. Using the

Corrected Geomagnetic Coordinates, the conjugate point to SANAE is located at [57°29'N 43°07'W $L = 4.3$] with MLTMN of 2.6 hrs near Greenland.

Figure 5.3.4 shows some lightning activities along the coast of Greenland, thus whistlers recorded at SANAE are mostly likely generated by lightning strikes at SANAE's conjugate point which lies close to Greenland.

From seasonal variation of whistlers at SANAE, Antarctica, it has been noted that they are highly likely to be observed from June to September because of better source and reception conditions. The ionosphere is more transparent to the passage of VLF waves at the receiver station during this time (winter at SANAE) and it is summer in the source region. Lightning conditions are most prevalent in summer at the source.

The diurnal percent probability of observing whistlers at SANAE greatly reduces during the day from that at night. This is due to attenuation of the VLF signal during the day in the D region as compared to at night when the D region disappears making the ionosphere more accessible to the passage of VLF waves and this is a confirmation of Helliwell [1965]. Helliwell noted that whistlers were more likely to be recorded during the night than during the day.

We can conclude that whistlers recorded at SANAE are probably generated by lightning recurring along the coastal areas of Greenland as this is the closest source to SANAE's conjugate point.

Greenland is a land of low lightning occurrence which would explain the low occurrence of whistlers at SANAE. In general it is noted that whistler activity decreases as one moves east in longitude from the stations SIPLE to HALLEY to SANAE.

SIPLE's conjugate lies in the east coast of North America where lightning activity is high. Halley's conjugate is off the coast of North America with lower lightning occurrence.

This leads us to the conclusion that in the main whistlers at a given station arise from lightning occurring very close to the station's conjugate point.

Chapter 6

ASD Index of VLF Activity

6.1 Introduction

VLF waves make an important contribution to the interactions and stability of particle populations in the magnetosphere. It is desirable therefore to have an index to represent the wave activity present at any given time. This index should not only give a measure of the intensity of the waves but also an indication of their character, in particular, the index should enable us to distinguish between chorus and hiss-like emissions. In this chapter we examine a simple way of doing this. This index should help to automate the study of ELF chorus and hiss.

The index we have devised has two elements, A, the Average Amplitude, and SD, the Standard Deviation, in time intervals of about 30s. We will call this the ASD index of VLF activity and we will discuss here its effectiveness by considering a number of case studies. We have used the index in two frequency ranges 2-2.5 kHz and 2.5-3 kHz; as at SANAE this is the frequency range in which chorus is observed.

The dominant emissions are chorus, hiss and sferics. Chorus consists of rising tones spaced in time, and hiss is generally a steady band of noise, both of which occur in a narrow range of frequencies. We also observe sferics, which are short duration (~ 2 ms) bursts occurring over a wide frequency range. The effect of sferics can be reduced by averaging over a time period (for example 30 s), see Figure 6.1.1, and we hope to differentiate between chorus and hiss because of their different variability.

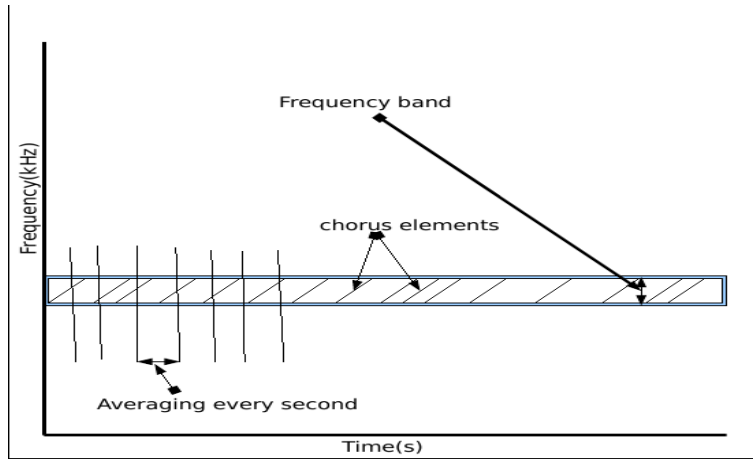


Figure 6.1.1: Generating the index

First let us examine the spectral characteristics of chorus and hiss. In Figure 6.1.2 and 6.1.3 we show typical power spectra for chorus and hiss. The chorus can be seen to extend from about 1.5 to 3.2 kHz and hiss extends from about 0.5 to 2.8 kHz. The lower cut-off frequency in the chorus is almost certainly due to a propagation cut-off in the earth-ionosphere waveguide whereas hiss extends down to 0.5 kHz suggesting that it enters the ionosphere close to SANA E and is not subject to the waveguide cut-off.

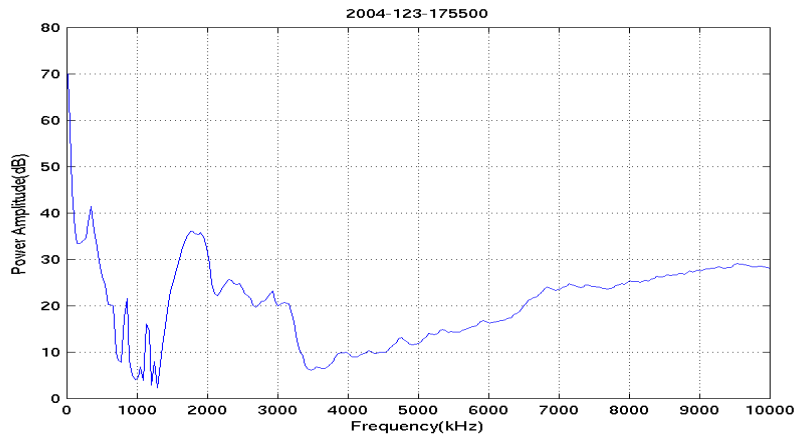


Figure 6.1.2: Chorus averaged power spectrum

The cut-off was obtained as follows:

$\frac{\lambda_c}{2} \approx h$, thus $\lambda_c = 200$ km because h in the earth-ionosphere wave guide is ~ 100 km ; Using the Equation below, we then computed the cut-off frequency.

$$c = f\lambda \tag{6.1.1}$$

where c is the speed of light in (km/s) thus giving $f_c = \frac{3 \times 10^5}{200} = 1.5$ kHz.

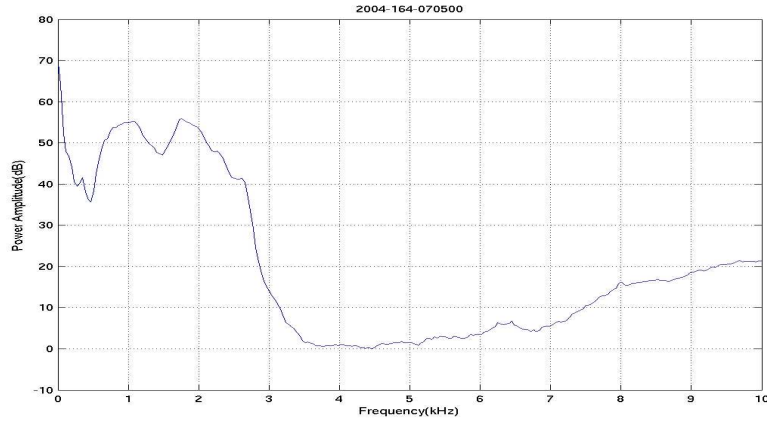


Figure 6.1.3: Hiss averaged power spectrum

It is clear that if we select frequencies in the range 2 to 3 kHz we will detect hiss and chorus when it occurs.

We now look at a sample of chorus recorded at SANAE and lasting 30s (Figure 6.1.4a) and plot the amplitude of the signal in a frequency band 2 to 2.5 kHz (Figure 6.1.4b). It can be seen that signal amplitude is variable between 0.2 and 0.4 volts (arbitrary units). Similar figures are given for hiss (Figures 6.1.5a and 5b).

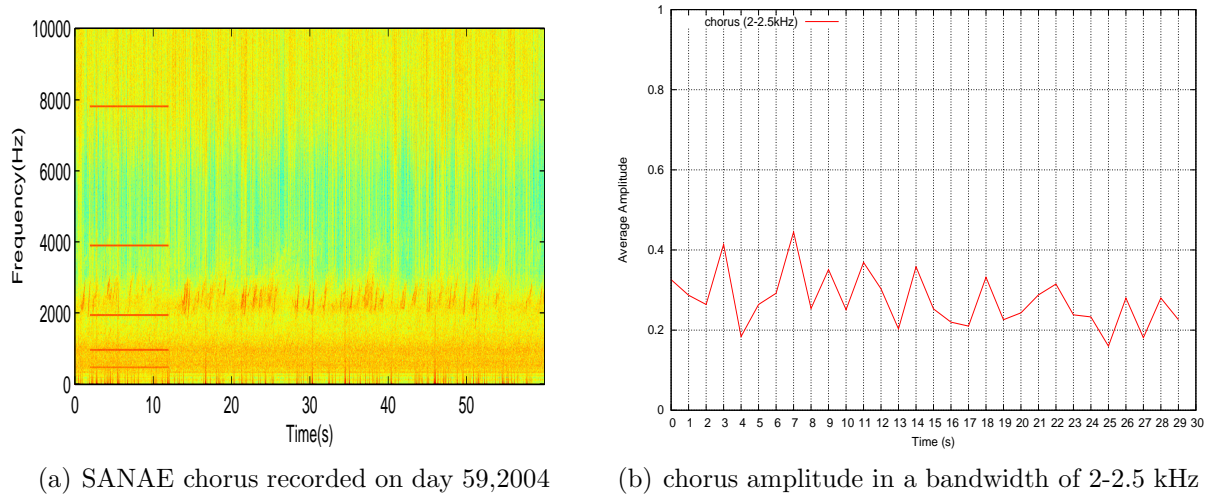


Figure 6.1.4: Chorus spectrogram & its amplitude recorded at SANAE on day 59,2004

A clear difference between the plots in Figures 6.1.4b and 6.1.5b is the time scale of the variability.

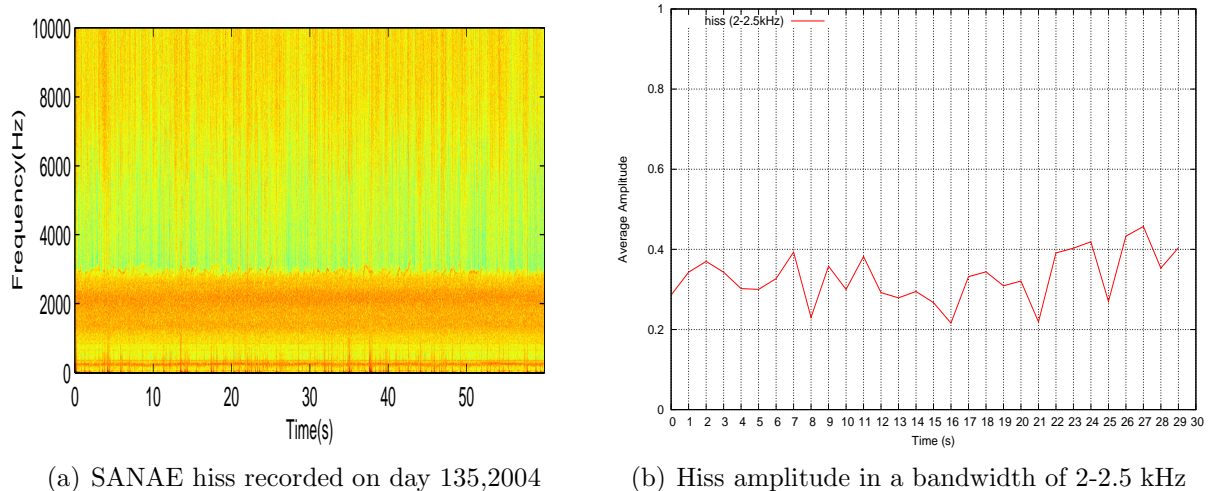


Figure 6.1.5: Hiss spectrogram and its amplitude recorded at SANA E on day 135, 2004

The question now is can the ASD index be used to distinguish between these two types of emission. To study this we have looked at chorus and hiss separately and derived values for the elements of the index. First we describe how the index is calculated.

The index was obtained from spectrograms in the following way. For each 30 ms spectrum the average amplitude across the chosen frequency band is calculated and then averaged for each 1 second interval in a 30 second time period. This yields a set of average amplitudes. The SD is then calculated by using the 1 second averages using the equation below.

$$SD = \sqrt{\frac{\sum_{n=0}^N (A_n - \bar{A})^2}{N}} \quad (6.1.2)$$

where $\bar{A} = \frac{\sum_{n=0}^N A_n}{N}$, and A_n is the average amplitude within a second, for $n = 0, 1, \dots, N$, and N is the number of average amplitudes (A_n) in 30 seconds, which is 30.

The index was then calculated for 25 cases with chorus present and 25 cases with hiss and the results are shown in Figure 6.1.6. In this figure it may be seen that chorus generally gives a lower average amplitude than hiss and has a larger SD. It is not clear that we can definitively identify chorus and hiss events from this index but we can use the index to give an indication as to whether the signal is hiss-like or chorus-like.

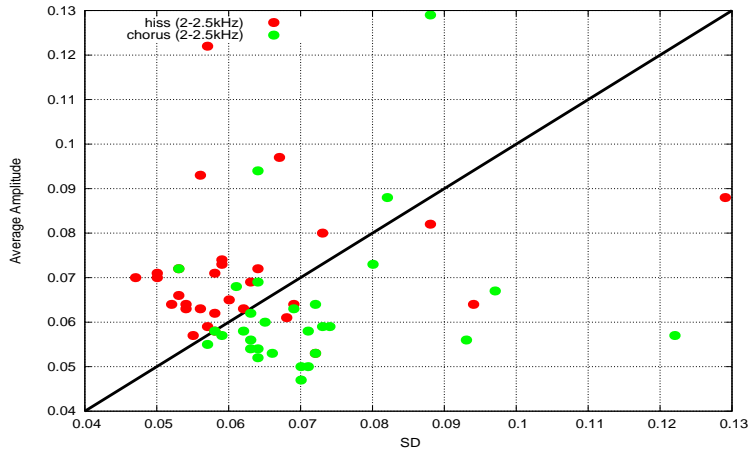


Figure 6.1.6: ASD index of VLF activity

To see how the index would vary for a number of wav files recorded at SANA E, we selected days on which chorus was more prevalent than any other VLF emission.

For the chorus case, chorus wav files from different days were selected and processed at two frequency bands as indicated above. We used chorus observed on days, 059, 070, 103 and 123 of the year 2004 because it is well defined.

The problem in doing this is that these different chorus wav files will have different intensities and will not clearly indicate the precise SD value for the chorus case, but just an indication of chorus being present.

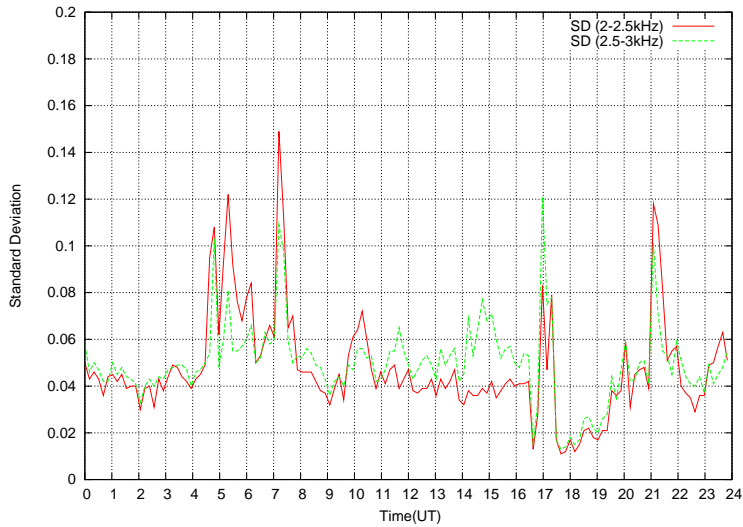


Figure 6.1.7: Chorus Case

Figure 6.1.7 shows the SD of chorus at different frequency bands for a period of

24 hours. The peaks in the figure are an indication of chorus being present. It was observed that they vary with frequency band and intensity of chorus observed at a particular time. The SD in this case varies between 0.02 and 0.2.

A similar procedure was done for the hiss case with hiss wav files from day, 022, 024, 027, 028, 030, 128, 129, 135 and 136 of 2004. It has been shown in Figure 6.1.8 that the SD of hiss is nearly constant from one wav file to the other. This is because of uniform characteristic spectral structure of hiss.

Figure 6.1.8 shows the SD for hiss. It is evident that the hiss' SD is nearly constant in all the hiss wav file because hiss is a relatively steady signal. This feature is characteristic of hiss and enables us to differentiate it from chorus and is considered to be a major indicator for the signature. It was observed that the SD varied above 0 but below 0.11 for this case.

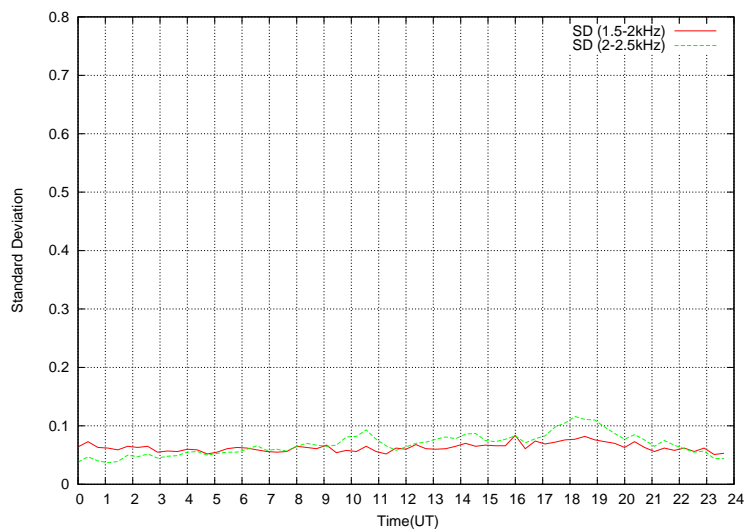


Figure 6.1.8: Hiss Case

We have used different frequency bands for hiss from that used for chorus because usually hiss is observed at a lower frequency band. As such in order to achieve a purely hiss case, we selected hiss at this band, thus eliminating any possible contamination due to polar chorus. This is chorus superimposed on hiss.

6.2 Advantages and Limitations of the Index

Even if we have not established precise SD values for chorus and hiss, the index has shown some degree of automating the study of VLF activities and as such VLF wav files can be processed without having to isolate chorus wav files from hiss when studying these emissions. For example, we processed wav files for day 275 of 2005 as shown in Figure 6.2.1. Refer to Figure 4.2.11 for the spectrogram. The peaks in the figure shows the presence of chorus and its SD varied between 0.02 and 0.1.

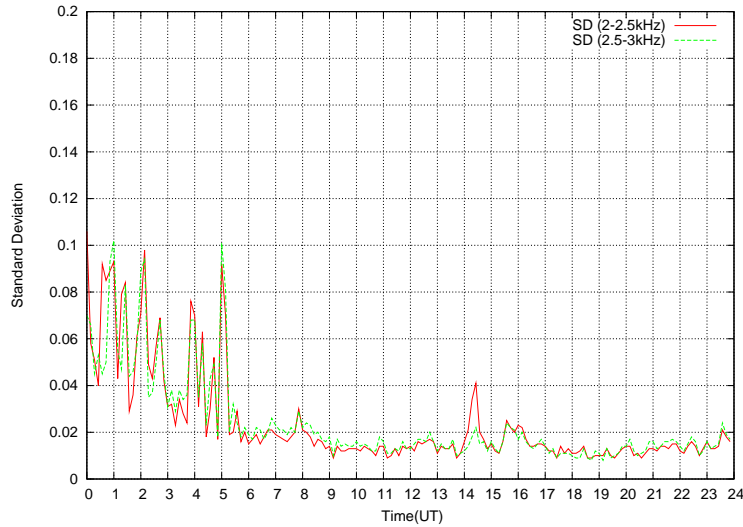


Figure 6.2.1: SD of VLF activity on day 275, 2005

Even though we have experienced complications in establishing the index, we feel that it will enable us to investigate for example if the observed absorption is due to hiss or chorus. Moreover, it is faster than the manual way explained in the case studies and also outputs the nature of the averaged spectrum for every wav file which helps in verifying the type of VLF signature from a particular wav file and indicates precisely, both the lower and upper boundary frequencies of a given emission (refer to Figures 6.1.2 and 6.1.3).

The index will fail when the location of the station where chorus is being observed with respect to the exit point is not in the dark. This means that chorus would occur but will not be recorded at a receiver station whose ionosphere is illuminated, because of greater attenuation of VLF waves in the ionosphere. This only applies to ground based observations, thus seasonal effects will be encountered in this case.

We have observed that the index varies from one frequency band to another. The results shown here were limited to 2 kHz and 3 kHz, because we mostly see chorus on these frequencies at SANAE.

6.3 Ionospheric Absorption versus the ASD Index

This section presents results for testing the ASD index of VLF Activity with ionospheric absorption at different L-values. The case studies presented in section 4.2 were done before the index was generated. We show how the index varies with ionospheric absorption limiting our time of absorption observation at the Finnish chain to darkness only for the reasons given earlier.

Figures presented here are in relation to the VLF chorus recorded on day 352 of 2004. Chorus was recorded from \sim 0348 UT to 0900 UT, however we have limited our time to 0000 UT and 0700 UT to eliminate masking of chorus enhanced absorption by solar effects during day time.

The hourly variation of the ASD index was established using VLF wave files recorded at SANAE as has been elaborated in section 6 above for this particular day and compared it to ionospheric absorption at the Finnish chain.

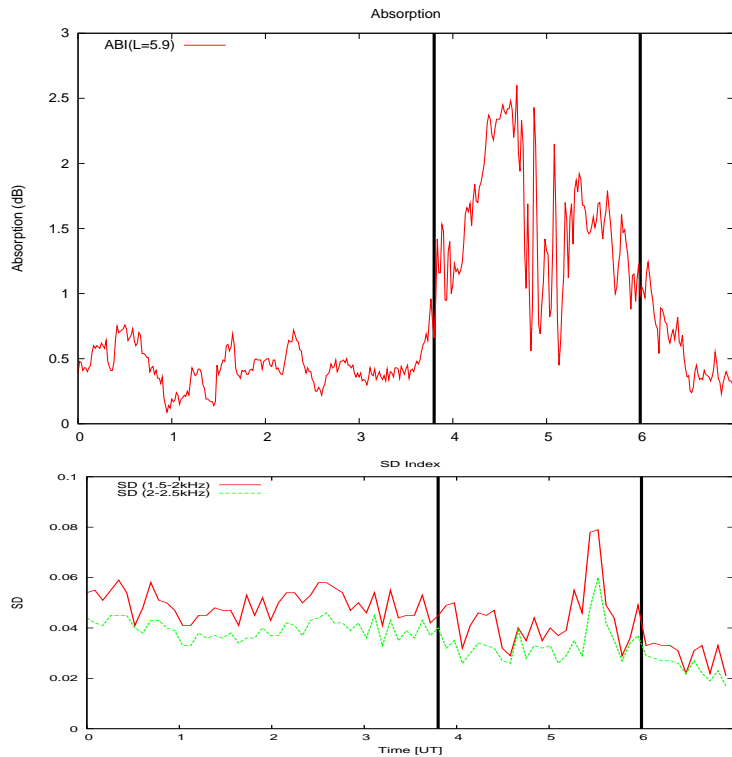


Figure 6.3.1: Absorption at Abisko, vs ASD Index at SANAE on day 352,2004.

Figure 6.3.1 shows how the index (at the bottom) varies with absorption (top) recorded at Abisko. The two vertical lines between 0348 UT and 0600 UT correspond to the time when chorus is observed on the quicklooks at SANAE. It is clear that there is a 2.2dB increase in absorption that does not coincide with the peak in the index. When compared to the chorus signal intensity, it was observed that the distinctive peak in absorption corresponded to a decrease in intensity of chorus as shown in Figure 6.3.2. This result is similar to that presented in the case studies.

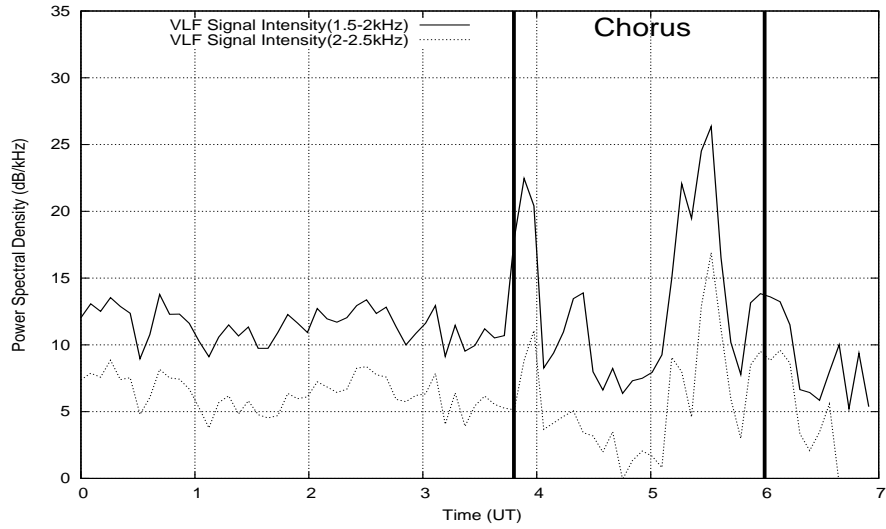


Figure 6.3.2: Power spectral density of the VLF signal on day 352,2004

The 0.06 SD peak corresponds to a ~ 20 dB/kHz increase in the chorus signal intensity between 1.5-2 kHz frequency band and a 13 dB/kHz increase in the intensity between 2-2.5 kHz band.

The nature of absorption at Ivalo also follows the variation of the index at SANAE at the same UT for an observation made on day 352 of 2004.

Figure 6.3.3 shows absorption recorded at Ivalo (top) at the same universal time when the index (bottom) is computed for day 352 VLF data recorded at SANAE.

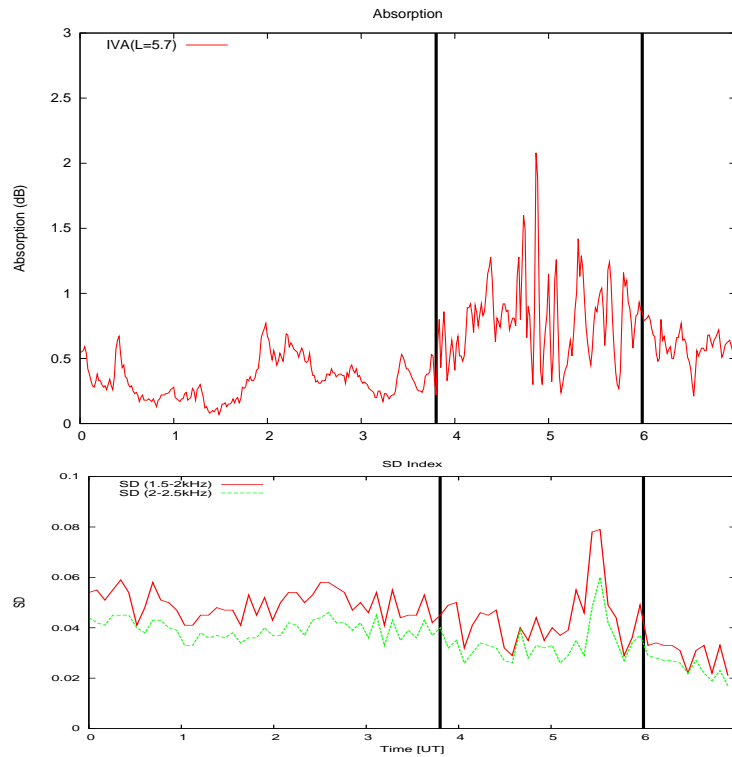


Figure 6.3.3: Absorption at Ivalo, vs ASD Index at SANAE on day 352, 2004

It is clear that absorption at Ivalo does not correlate to the index. This is similar to earlier results and this observation is possible because of the shift in the magnetic longitude of the Finnish chain from SANAE's CP.

Moreover, the reception conditions at SANAE are not favorable because it is summer at SANAE for this period of the year. Hence the reception of VLF waves is not favorable because SANAE is mostly illuminated for a greater part of the day. Referring to Figure 5.2.7(b), we indeed see that the percent probability of observing chorus in December at SANAE is less than 20%.

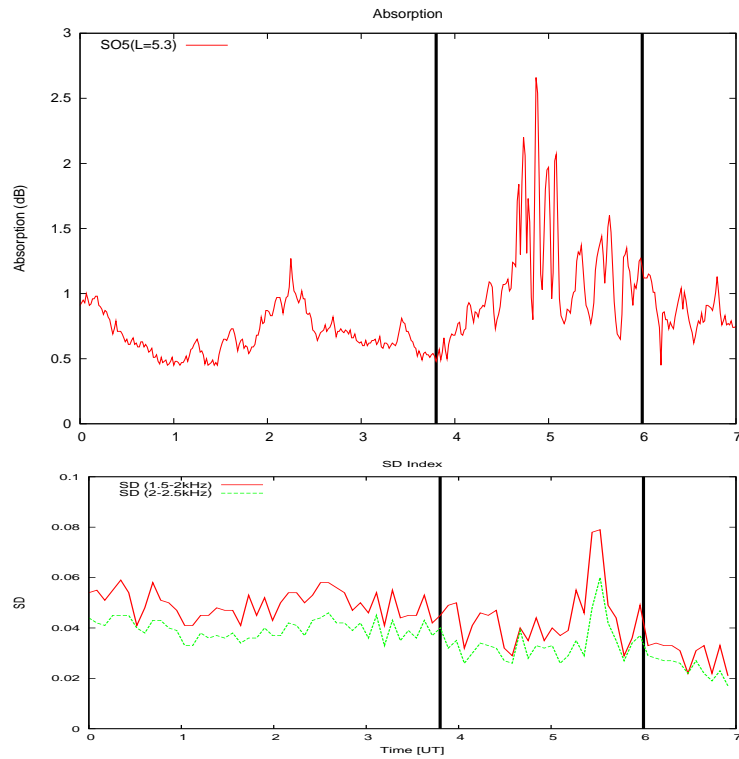


Figure 6.3.4: Absorption at Sodankylä, vs ASD Index at SANA E on day 352,2004.

Figure 6.3.4 shows how absorption at Sodankylä varies with the index measured on day 352 of 2004 from 0000 UT to 0700 UT. As at Ivalo and Abisko, the peak in absorption does not correlate to the peak in the index.

The Figure 6.3.5 below shows how absorption at Rovaniemi varies with the index at SANAE for day 352 of 2004. The period of observation is from 0000 UT to 0700 UT and the vertical lines limit our observation to the time when chorus is recorded at SANAE and to darkness at the Finnish chain.

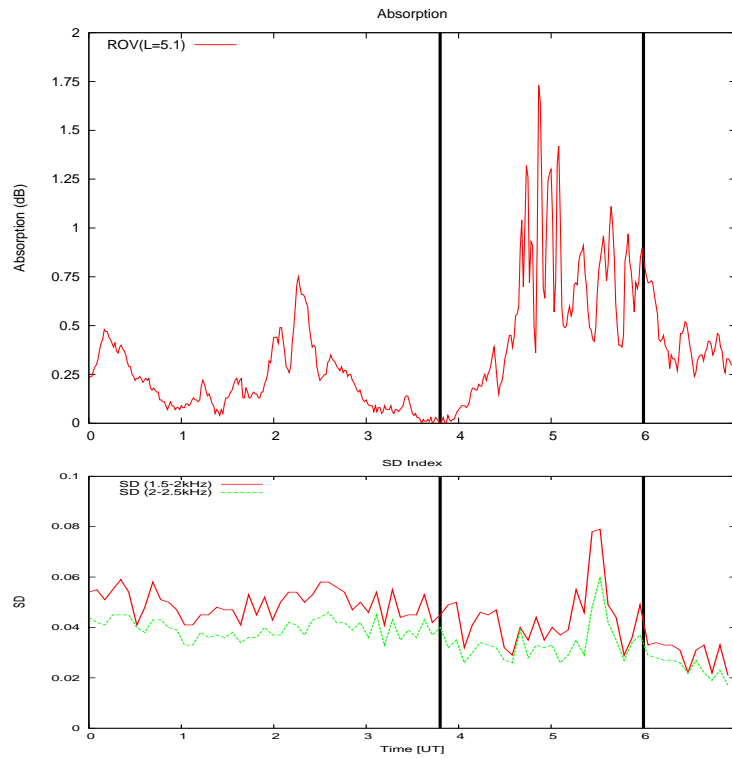


Figure 6.3.5: Absorption at Rovaniemi, vs ASD Index at SANAE on day 352,2004

There is a 1.3 dB increase in absorption at Rovaniemi which does not correspond to the peak in the SD. This absorption is lower than that recorded at stations with L-value higher than Rovaniemi for the same period of observation, i.e (0348-0600 UT) when chorus is observed at SANAE. The VLF signal intensity varies as before.

Figure 6.3.6 shows absorption at Oulu and its variation with the index on day 352 of 2004. There is a dramatic difference in absorption recorded between the two vertical lines with the rest of the stations. There is a 0.4 increase in absorption as compared to a > 1 dB increase at the other stations, but does not also relate to the peak in the index.

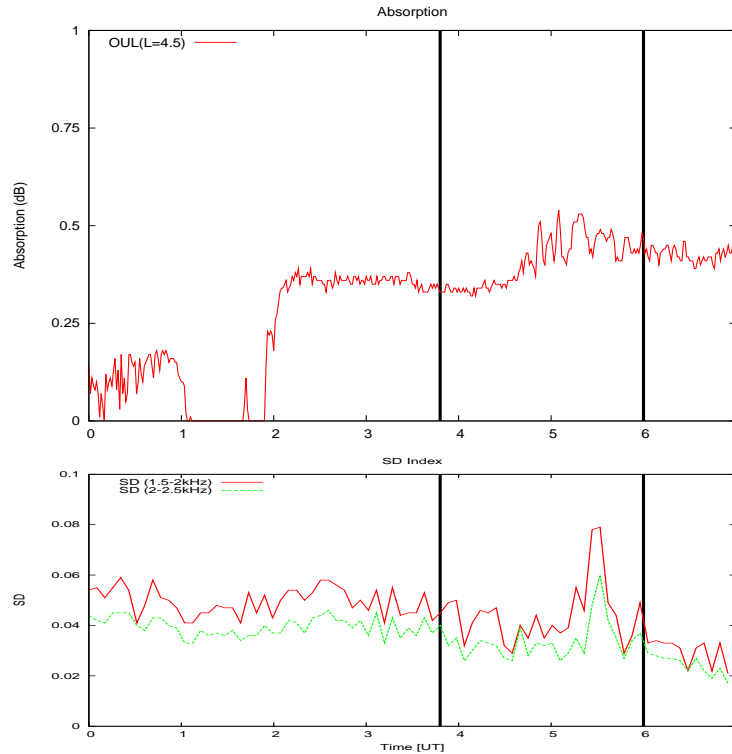


Figure 6.3.6: Absorption at Oulu, vs ASD Index at SANAE on day 352,2004.

As in section 4.2, none of the results presented here show a correlation of absorption and the index for the same reasons given before.

Chapter 7

Conclusion

7.1 Introduction

There is an observed increase in particle flux in the magnetosphere at lower energies. Thus, for a given emission frequency ω along a given magnetic field line, we anticipate to have the highest contribution from electrons with the lowest energy which satisfies the equation (7.1) below [Hargreaves, 1979]. Equation (7.1) implies that particles with large parallel velocities will resonate with low frequency waves and those with smaller parallel velocities will resonate with high frequency waves.

$$W_{\parallel} = \frac{B^2}{2\mu_0 N} \frac{\Omega}{\omega} \left(1 - \frac{\omega}{\Omega}\right)^3 \quad (7.1)$$

It can be concluded from Figure (7.1) that the energies observed at lower and higher L - values are because the magnetic field is inversely proportional to the radial distance r raised to the power of three as shown in equation (7.2).

$$B \propto \frac{1}{r^3} \quad (7.2)$$

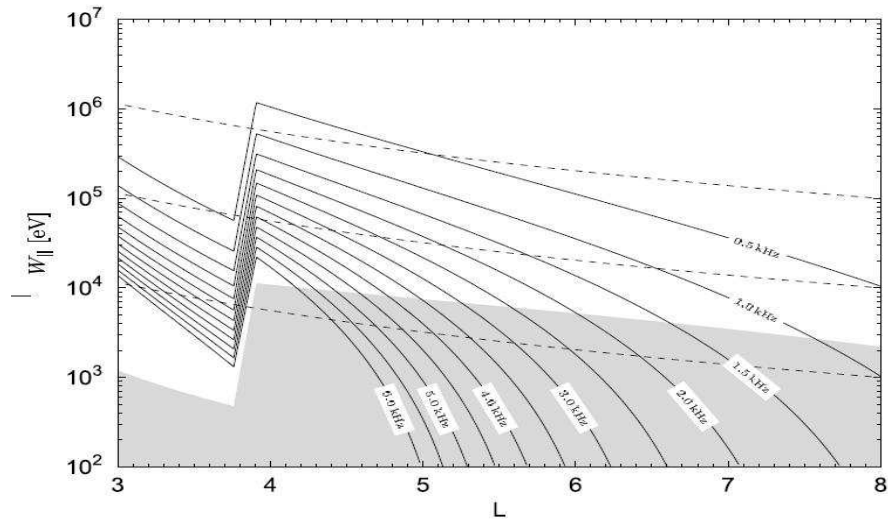


Figure 7.1: Resonant Parallel Energies vs L - value [Smith et al, 1996 Figure 10].

7.2 Discussion

In chapter 4, we presented case studies using two assumptions:

1. We may be able to observe enhanced absorption at the Finnish chain at the same MLT as chorus recorded at SANAE. This was referred to as first method and was marked A.
2. Enhanced absorption (marked B) may be recorded at the Finnish chain at the same universal time when chorus is recorded at SANAE, implying that the chorus observed at SANAE would have spread eastwards crossing the longitude passing Finland, thereby inducing electron precipitation at the same UT.

Even though we can not conclude that there is a correlation between absorption at the Finnish chain and chorus at SANAE, we have times when absorption increases and decreases with the switching on and off of chorus at the same UT. Chorus recorded at SANAE shows some indication of spreading in longitude to Finland's. This follows from a number of cases when we have seen absorption at the same UT when chorus is recorded at SANAE, but it is not always the case.

It was observed that the first method did not show any correlation between chorus and absorption, this may be due to the shift in the longitude of the Finnish chain from SANAE, meaning that SANAE and the Finnish stations are observing events on field lines that link with different regions of the magnetosphere.

Enhanced absorption was observed to increase with an increase in the L-value, and using Smirnova, (1984), we calculated the L-value for the source region and we noted that it was higher than SANAE's L-value. This result made us interpret the observation in terms of the movement of the interaction region from lower to higher L-shells which explains the increase in absorption at higher L-shells.

If the assumption made in chapter 4 is true, it is suggested that the observed increase in absorption with increasing L-value may also be attributed to:

1. Reduced parallel resonant energies.
2. and possibly a smaller recombination time on higher L-value.

It can be concluded from the Chapter 5 that:

1. Chorus recorded at SANAE predominantly occurs between 0600 UT to 1300 UT and mostly between 2-3.9 kHz.
2. The diurnal variation of chorus has been observed to have a peak between 0800 UT and 0900 UT for all the three years' VLF data worked on. It was observed that the percent probability of recording chorus was higher in 2004 than 2002 and 2005. This observation corresponded to the increase in the Dst index, which indicates that chorus is highly observed with an increase in the radiation belt electrons.

Moreover, Figure (5.2.1) shows the magnetic field in the noon-midnight meridian plane based on the magnetosphere field model of Mead and Fairfield, (1975). The regions in which chorus is thought to be produced are noted by dots. Near midnight, chorus is generated close to the magnetic equator by substorm-injected electrons from the plasma sheet. Chorus activity increases in the dawn to noon sector due to the azimuthal drift of energetic electrons towards dawn. This enhances energetic electron flux which consequently enhances wave-particle interaction in the postmid-night sector. This can also be seen from the diurnal variation in Figures (5.2.6), (5.2.7) and (5.2.8). On the dayside at large L values, chorus is also generated over a much larger span of magnetic latitudes. Within $1-2R_E$ of the magnetopause, chorus may originate in minimum magnetic B pockets, which are local regions of minimum magnetic field strength that occur at high latitudes as a result of the solar wind compression of the dayside magnetosphere [Tsurutani and Lakhina, 1997].

From section 5.3, we observed an increase in the diurnal probability of recording whistlers at SANAE from dusk to dawn. This is highly likely to correspond to increase in lightning in the conjugate hemisphere. The seasonal variation of whistlers at SANAE is evidently high in winter months. This is because in winter, SANAE is in the dark, making the ionosphere more accessible to the reception of VLF waves. Moreover, it is summer in the northern hemisphere, which offers better source conditions (i.e lightning strikes are most prevalent in summer).

We can conclude that whistlers recorded at SANAE are probably generated by lightning recurring along the coastal areas of Greenland as this is the closest source to SANAE's conjugate point.

Greenland is a land of low lightning occurrence which would explain the low occurrence of whistlers at SANAE. In general it is noted that whistler activity decreases as one moves east in longitude from the stations SIPLE to HALLEY to SANAE.

It has been observed that chorus and hiss have different averaged spectra and these were used to identify the signatures as has been shown in Figures 6.1.2 and 6.1.3 respectively. Moreover, their average amplitudes vary with frequency band as can be seen in the Table 7.1 on page 75.

VLF hiss has high averaged amplitudes in 1-2.5 kHz frequency bands and its amplitude drops from 2.5 kHz to higher frequency bands. The decrease may be described as having a negative gradient in observing the signature. Chorus on the other hand has a low averaged amplitude in the 1.5-2 kHz frequency band, and has a high averaged amplitude between 2-4 kHz and drops beyond 4 kHz.

The observed amplitudes of chorus, hiss and sferics at various frequencies suggest that hiss will be observed at lower frequencies as opposed to higher frequencies. Chorus has a normal distribution of being observed at about 2.5 kHz whereas sferics are most prevalent at frequencies greater than 4 kHz.

AVERAGE AMPLITUDES OF VLF EMISSIONS			
	1.5-2 kHz	2-2.5 kHz	2.5-3 kHz
Chorus	28.31	28.19	22.01
Hiss	44.31	44.89	29.34
sferic	20.85	24.40	30.91

Table 7.1: Average amplitudes of VLF emissions at different frequency bands

There is no positive correlation between the ASD index at SANAE and enhanced absorption at the Finnish chain as shown in section 6.3.

It was difficult to come up with a standard ASD value for chorus and hiss, however we have been able to show that the chorus SD varies widely, and that for hiss, it is almost constant. Refer to Figures 6.1.7 and 6.1.8 respectively.

A relationship between chorus and absorption was not found as such the proposed ASD index of VLF activity does not describe the relationship between chorus and absorption but only acts as an indicator for the presence or absence of chorus and hiss, refer to Figure 6.2.1. The figure shows SD part of the index at two frequency bands on day 275 of 2005 indicating the presence of chorus at various peaks ranging from 0.02 and 0.1. Refer to Figure 4.2.11 for the spectrogram.

We have not fully achieved the aim of our study because of the complexity of the investigation. The Finnish chain is shifted in longitude from SANAE's CP. Using the two methods in studying absorption as explained earlier, we still can not conclude much from our investigation. But we noted that:

1. Increased absorption occurs at an MLT when the probability of chorus occurring is high; the maximum absorption in case 1, for example, occurs between 0400 and 0500 UT and this at the Finnish chain corresponds to about 0600 and 0700 MLT.
2. Absorption varies in longitude in a way that might correspond to the switching on and off of chorus.

We therefore propose that, to effectively see if enhanced absorption at the Finnish chain was due to chorus recorded at SANAE, statistical methods should be applied. Absorption statistics should be made at different Finnish stations and compared with chorus statistics at SANAE.

Secondly, to quantitatively and effectively study chorus and ionospheric absorption, data from exactly conjugate stations should be used. This would help in observing events on field lines that link to the same regions of the magnetosphere. If there is no such data available then we propose that there be VLF receivers in the southern hemisphere which are exactly conjugate to riometers in the northern hemisphere and vice versa.

Bibliography

- [1] Baker, D. N., Coupling between the solar wind, Magnetosphere, Ionosphere and Neutral Atmosphere, University of Colorado, Boulder, CO 80309, 2004.
- [2] Bob, A and Thorne, R. M., Modelling Energetic Electron Precipitation near the south African Anomaly, *Journal of Geophysical Research*, 104(A4), 7037-7044, 1999.
- [3] Brice, N. M., An explanation of triggered very low frequency emissions, *Journal of Geophysical Research*, 68, 4626, 1963.
- [4] Brice, N. M., Discrete VLF emissions from the upper atmosphere, SEL-64-088, Radiosci Lab, Stanford Electron Lab, Stanford University, Stanford, California, 1964a.
- [5] Brice, N. M., Fundamentals of very low frequency emission generation mechanisms, *Journal of Geophysical Research*, 69, 4515, 1964b.
- [6] Carpenter, D. L., Whistler evidence of a 'Knee' in the magnetospheric ionisation density profile, *Journal of Geophysical Research*, 68(6), 1675-1682, 1963.
- [7] Collier, A. B., VLF and ULF Waves Associated with Magnetospheric Substorms, 2006: a PhD thesis.
- [8] Davies, K., Ionospheric radio, A book published by Peter Peregrinus Ltd, London, United Kingdom, 1990.
- [9] Dowden, R. L., Doppler-shifted cyclotron radiation from electrons., A theory of very low frequency emissions from the exosphere, *Journal of Geophysical Research.*, 67, 1745, 1962.
- [10] Drevin G. R., Stoker P. H., Riometer quiet day curves determined by the maximum density method, *American Geophysical Union*, 25(6), 1159-1166, 1990.

- [11] Ecklund, W. L., J. K. Hargreaves, and J. H. Pope., On the relation between auroral radio absorption and very low frequency emissions, *Journal of Geophysical Research*, 70, 4285, 1965.
- [12] Gary, S. P., What is a Plasma instability?, *Eos Trans American Geophysical Union*, 73, 529, 1992.
- [13] Gill, R. D., *Plasma Physics and Nuclear Fusion Research*, Academic, San Diego, California, 1981.
- [14] Gingauz, K. I., The Structure of the ionized gas envelope of the earth from direct measurements in the U.S.S.R. of local charged particle concentrations, *Planetary and Space Science*, 11(3), 281-296, 1963.
- [15] Hanson, W. B., Ed. F. S. Johnson., Structure of the Ionosphere, p.20 *in Satellite Environment Hand-book*, Stanford University Press, 1965.
- [16] Hargreaves, J. K., *The Upper Atmosphere and Solar Terrestrial Relations*, 1979. A book published by Van Nostrand Reinhold Company.
- [17] Hargreaves, J. K., *The solar-terrestrial environment*, Cambridge Atmospheric and Space Science Series, Cambridge University Press, 1992.
- [18] Hathaway, D. H and R. M. Wilson., Geomagnetic activity indicates large amplitude for sunspot cycle 24, *Geophysical Research Lett*, in press, 2006.
- [19] Hayakawa, M., Y. Yamanaka, M. Parrot, and F. Lefeuvre., The Wave Normals of Magnetospheric Chorus Emissions Observed on Board GEOS 2, *Journal of Geophysical Research*, 89(5A), 2811-2821, 1984.
- [20] Helliwell, R. A., *Whistlers and Related Ionospheric Phenomena*, Stanford University Press, 1965.
- [21] Helliwell, R. A., A theory of discrete VLF emissions from the magnetosphere, *Journal of Geophysical Research*, 72, 4773-4790, 1967.
- [22] Helliwell, R. A., Intensity of discrete VLF emissions, *in Particles and Fields in the Magnetosphere*, edited by B. M. McCormack, p. 292, D. Reidel, Hingham, Mass, 1970.

- [23] Helliwell, R. A., and T. L. Crystal, A feedback model of cyclotron interaction between whistler mode waves and energetic electrons in the magnetosphere, *Journal of Geophysical Research.*, 78, 7357, 1973.
- [24] Horne, R. B. and R. M. Thorne, Relativistic electron acceleration and precipitation during resonant interactions with whistler-mode chorus, *Geophysical Research letters*, 30(10), 34-1-34-4, 2003.
- [25] Insenberg, P. A., H. C. Koons, and J. F. Fennell., Simultaneous Observations of Energetic Electrons and Dawnside Chorus in Geosynchronous Orbit, *Journal of Geophysical Research*, 87(A3), 1495-1503, 1982.
- [26] Kennel, C. F., and H. E. Petscheck, Limit on stably trapped particle fluxes, *Journal of Geophysical Research.*, 71, 1, 1966.
- [27] Lefeuvre, F., T. Neubert, and M. Parrot, Wave Normal Directions and wave Distribution Functions for Ground-Based Transmitter Signals Observed on GEOS 1, *Journal of Geophysical Research*, 87(A8), 6203-6217, 1982.
- [28] Liemohn, H. B., Cyclotron resonance amplification of VLF and ULF whistlers, *Journal of Geophysical Research.*, 32, 39-55, 1967.
- [29] Lyons, L. R., and D. J. Williams, *Quantitative Aspects of Magnetospheric Physics*, D. Reidel, Norwell, Mass., 1984.
- [30] Matsumoto, H., and I. Kimura., Linear and nonlinear cyclotron instability and VLF emissions in the magnetosphere, *Planet Space Sci.*, 19, 567, 1971.
- [31] McNamara, L. F., *The ionosphere: Communication, surveillance and direction finding*, A book published by Kriegner publishing company, Malabar, Florida, 1991.
- [32] Mead, G. D., and D. H. Fairfield., A quantitative magnetospheric model derived from spacecraft magnetometer data, *Journal of Geophysical Research.*, 80, 523, 1975.
- [33] Nashimo, M., S. Nozawa and J. A. Holtet, Day time Ionospheric Absorption Features in the Polar Cap Associated with Poleward Drifting F-region Plasma Patches, *Earth Planets Space*, 50, 107-117, 1998.
- [34] Nunn, D., A theory of VLF emissions, *Planet Space Sci.*, 19, 1141, 1971.

- [35] Nunn, D., A self consistent theory of triggered VLF emissions, Planet Space Sci., 22, 349, 1974.
- [36] Østgaard, N., J. Stadsnes, J. Bjordal, E. Thorsen, R. Vondrak R., S. A. Cummer, D. L. Chenette, G. K. Parks, M. J. Brittnatcher and D. L. McKenzie, Global Scale Electron Precipitation During Substorm Expansions, Journal of Geophysical Research, 104(10), 191-204, 1999.
- [37] Ranta, H., A. Ranta and T. J. Rosenberg., The day to night ratio in auroral and subauroral zone riometer measurements during auroral absorption, Journal of Atmospheric and Terrestrial Physics, 46, 395-398.
- [38] Resenberg, T. J., R. A. Helliwell and J. P. Katsufakis, Electron Precipitation associated with discrete Very low frequency emissions, Journal of Geophysical Research, 76, 8445, 1971.
- [39] Roederer, J. G., Dynamics of Geomagnetically Trapped Radiation, Springer-Verlag, New York, 1970.
- [40] Santolik, O., D. A. Gurnett, J. S. Pickett, M. Parrot, and N. Cornilleau-Wehrlin., Central position of the source region of storm-time chorus, Planetary and Space Science, 53, 299-305, 2005.
- [41] Sazhin, S. S. and M. Hayakawa, Magnetospheric Chorus Emissions, A Review, Planetary and Space Science, 40(5), 681-697, 1992.
- [42] Sørass, F., R. H. Lindalen, K. Måseide, A. Engeland, T. A. Sten, and D. S. Evance., Proton precipitation and the H_{β} emission in a post breakup auroral glow, Journal of Geophysical Research, 79, 1851-1859, 1974.
- [43] Stern, D. and M. Peredo., The exploration of the magnetosphere, 1995, <http://www-spf.gsfc.nasa.gov/Educational/wradbelt.html>
- [44] Storey, L. R. O., An Investigation of Whistling Atmospheric, Philosophical Transactions of the Royal Society, A-246, 113-141, 1953.
- [45] Sudan, R. N., and E. Ott, Theory of triggered VLF emissions, Journal of Geophysical Research, 76, 4463, 1971.

- [46] Tivota, E. E., Kozelov, B. V., F. Jiricek, J. Smilauer, A. G. Demekhov, and V. Yu. Trakhtengerts., Verification of the backward wave oscillator model of VLF chorus generation using data from MAGION 5 satellite, *Annales Geophysicae*, 1073-1081, 2003.
- [47] Thorne, R. M. and C. F. Kennel., Relativistic electron precipitation during magnetic storm main phase, *Journal of Geophysical Research*, 76(A7), 4446, 1971.
- [48] Trakhtengerts, V. Y., Magnetosphere cyclotron maser: Backward wave oscillator generation regime, *Journal of Geophysical Research*, 100(A9), 17205 - 17210, 1995.
- [49] Tsurutani, B. T. and E. J. Smith., Postmidnight Chorus: A Substorm Phenomenon, *Journal of Geophysical Research*, 79(1), 112-127, 1974,
- [50] Tsurutani, B and E. Smith., Two types of magnetospheric ELF chorus and their substorm dependancies, *Journal of Geophysical Research*, 82(32), 5112-5128, 1977.
- [51] Tsurutani, B. T., and G. S., Lakhina., Some Basic Concepts Of Wave-Particle Interactions in Collionless Plasmas, *American Geophysical Union*, 35, 491-505, 1997.
- [52] Wang, Z., T. J. Rosenberg, P. Stauning, S. Basu, and G. Crowley., Calculation of Riometer Absorption Associated with F-region Plasma Structures based on Sondre Stromfjord Incoherent Scatter Radar Observation, *Radio Science*, 29, 209-215, 1994.
- [53] Yahnin, A. G., T. A. Yahnina, and A. G. Demekhov., The VLF and ULF related Particle Precipitations and Cold Plasma Structures in the Equatorial Magnetosphere, in *Physics of Auroral phenomena 2003*, Proc. XXVI Annual Seminar, Apatity, 131-134, Kola Science center, Russian Academy of Science, 2003.
- [54] Walker, A. D. M., *Plasma in the Magnetosphere*, Spring-Verlag, 1993.